# Pathophysiological changes in the hippocampus in a murine model of episodic ataxia type 6

Inaugural-Dissertation

zur Erlangung des Doktorgrades
der Mathematisch-Naturwissenschaftlichen Fakultät
der Heinrich-Heine-Universität Düsseldorf

vorgelegt von

**Iuliia Kolobkova**
aus Sankt Petersburg (Russische Föderation)

**Jülich, Februar 2020**

aus dem Institut für Biologische Informationsprozesse –

Molekular- und Zellphysiologie des Forschungszentrums Jülich

Gedruckt mit der Genehmigung der

Mathematisch-Naturwissenschaftlichen Fakultät der

Heinrich-Heine-Universität Düsseldorf

Referent: Prof. Dr. Christoph Fahlke

Korreferent: Prof. Dr. Christine R. Rose

Tag der mündlichen Prüfung:

*Dedicated to my family*

# Contents

## List of figures

**List of tables**

# 1 Abstract

Glial glutamate uptake is essential for a fast reduction of the extracellular glutamate concentration in the synaptic cleft. It determines the time course of glutamatergic neurotransmission and prevents neuronal excitotoxicity.

Mutations in *SLC1A3* – that encodes the glial excitatory amino acid transporter 1 (EAAT1/GLAST) – are associated with episodic ataxia type 6 (EA6). A mutation causing the exchange of proline by arginine at position 290 (P290R) was found in a patient with EA6 suffering from ataxia and epileptic seizures. EAAT1/GLAST functions as glutamate transporter and as anion channel, and P290R has been shown to impair glutamate transport, while enhancing anion channel activity.

To understand how such changes in EAAT1/GLAST function can lead to epilepsy, a knock-in mouse model (*Slc1a3*$^{P290R/+}$) was generated. Mutant mice exhibit impaired motor coordination and epileptic seizures. EAAT1/GLAST is highly expressed in hippocampal neural progenitor cells (NPCs) – glial cells, which are tightly functionally and spatially coupled to granule cells. Increased anion efflux from NPCs results in lower $[Cl^-]_{int}$ and might alter ambient GABA levels by increasing the driving force of the glial $Na^+/Cl^-$-dependent GABA transporter 3 (GAT-3).

Electrical recordings from granule cells show that inhibitory tonic GABA-mediated $Cl^-$ currents are decreased in *Slc1a3*$^{P290R/+}$ mice while the current amplitudes and frequencies of miniature inhibitory postsynaptic currents (mIPSCs) are unchanged. The reduced tonic inhibition is accompanied by an increase in AMPA receptor-mediated miniature excitatory postsynaptic currents (mEPSCs) in hippocampal neurons.

My work demonstrates an imbalance between excitatory and inhibitory neurotransmission that likely contributes to hippocampal hyperexcitatbility of EA6.

# 2 Zusammenfassung

Die gliale Aufnahme von Glutamat ist essentiell für die schnelle Reduktion der extrazellulären Glutamatkonzentration im synaptischen Spalt. Sie bestimmt den Zeitverlauf der glutamatergen Neurotransmission und verhindert eine neuronale Exzitotoxizität.

Mutationen im menschlichen Gen *SLC1A3*, das für den glialen exzitatorischen Aminosäure Transporter 1 (EAAT1/GLAST) kodiert, verursachen die Episodische Ataxie Typ 6 (EA6). Eine dieser Mutationen, die den Austausch von Prolin durch Arginin an Position 290 (P290R) verursacht, wurde in einem Patienten mit EA6 gefunden, der an Ataxie und epileptischen Krämpfen litt. EAAT1/GLAST kann sowohl als Glutamattransporter als auch als ein Anionenkanal funktionieren, und es konnte gezeigt werden, dass P290R den Glutamattransport beinträchtigt und die Anionenkanalaktivität erhöht.

Um zu verstehen, wie derartige Änderungen der EAAT1/GLAST Funktionen Epilepsie verursachen, wurde ein Knock-in Mausmodell (*Slc1a3*$^{P290R/+}$) entwickelt. Die Mäuse weisen eine beeinträchtigte motorische Koordination und epileptische Krämpfe auf. EAAT1/GLAST ist in hippokampalen neuralen Vorläuferzellen (NPCs) stark exprimiert. NPCs sind gliale Zellen, die stark an Körnerzellen gekoppelt sind. Ein erhöhter Efflux von Anionen aus NPCs könnte den umgebenden GABA Spiegel, durch eine Erhöhung der Triebkraft des $Na^+/Cl^-$-abhängigen GABA Transporter 3 (GAT-3), verändern.

Elektrophysiologische Experimente an Körnerzellen zeigen, dass die inhibitorische tonische GABA-vermittelten $Cl^-$ Ströme von *Slc1a3*$^{P290R/+}$ Mäusen reduziert sind, dies ist wahrscheinlich auf einen reduzierten extrazellulären GABA-Spiegel zurückzuführen. Gleichzeitig sind die Stromamplituden und die Frequenzen von inhibitorischen postsynaptischen Miniaturströmen (mIPSCs) unverändert. Die Reduktion der tonischen Inhibition geht mit einem Anstieg der AMPA Rezeptor-vermittelten exzitatorischen postsynaptischen Miniaturströme (mEPSCs) in hippokampalen Neuronen einher. In dieser Arbeit zeige ich zum ersten Mal ein Ungleichgewicht zwischen exzitatorischen und inhibitorischen Strömen, das vermutlich zur Hyperexzitabilität bei EA6 führt.

# 3 Introduction

Neurons interact through synapses. In chemical synapses neurotransmitters released by a presynaptic neuron bind to receptors on the membrane of a postsynaptic neuron and transmit a signal that can either be stimulating or inhibiting, depending on the type of neurotransmitter and receptor involved. The excitatory amino acid (EAA) glutamate is the major excitatory neurotransmitter in the central nervous system. Changes in glutamatergic neurotransmission are known to be implicated in numerous brain functions as well as in the pathogenesis of many neurological disorders, such as Alzheimer's disease, stroke, multiple sclerosis and epilepsy (Zhou and Danbolt, 2013; Vandenberg and Ryan, 2013; Jensen et al., 2015). Tight regulation of extracellular glutamate levels is essential for proper synaptic transmission and normal neuronal function.

## 3.1 Excitatory amino acid transporters (EAATs)

EAATs transport glutamate from the synaptic cleft into neural and glial cells and thus prevent its spillover beyond the synapse. Under physiological conditions, they can maintain a $10^6$-fold glutamate concentration gradient across the cell membrane (Zerangue and Kavanaugh, 1996). EAATs mediate the stoichiometrically coupled antiport of one glutamate, one proton and three sodium ions against one potassium ion (Levy et al., 1998; Zerangue and Kavanaugh, 1996), which results in a net positive charge movement (Bergles and Jahr, 1997). EAATs also function as anion-selective channels. Anion channel opening transitions are thought to only occur from intermediate states of the glutamate transport cycle (Machtens et al., 2015).

The mammalian EAAT family consists of five members with the human EAAT1–5 subtypes corresponding to GLAST, GLT-1, EAAC1, EAAT4, and EAAT5 in rodents (Danbolt, 2001, Fig. 3.1).

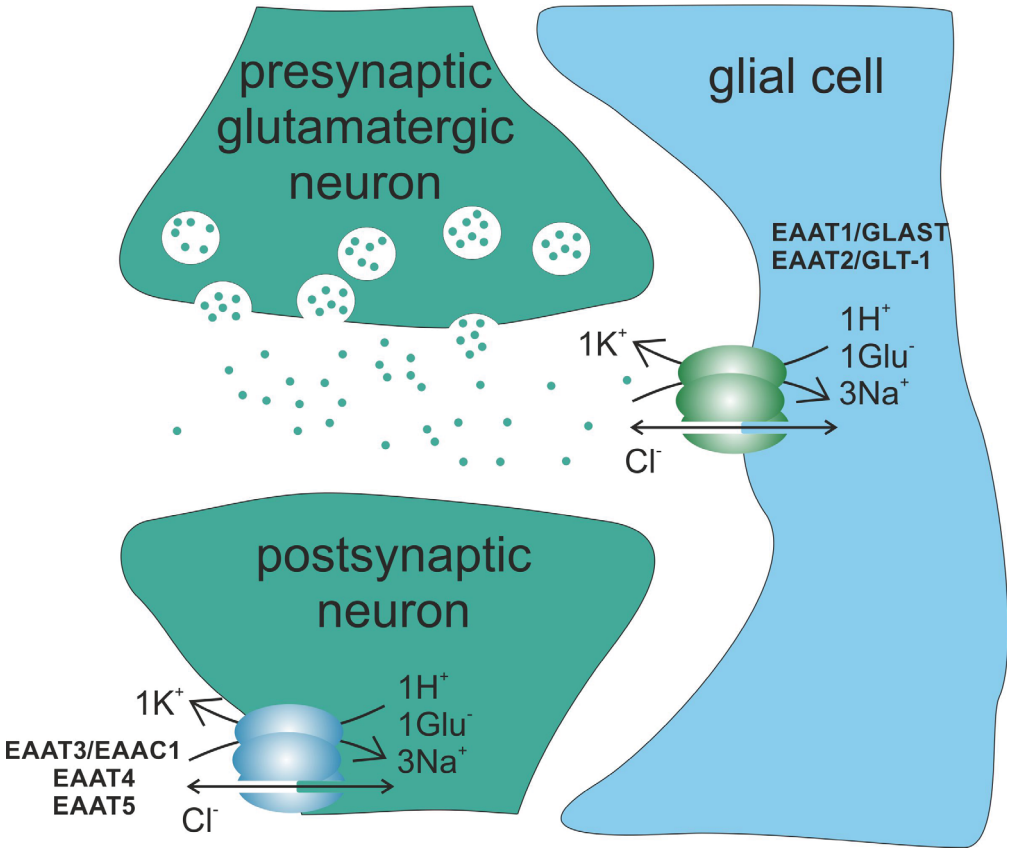


Figure 3.1: **Types of excitatory amino acid transporters at the glutamatergic synapse.** Glutamate transporters in glial cell plasma membranes EAAT1/GLAST, EAAT2/GLT-1 and neuronal isoforms EAAT3/EAAC1, EAAT4, EAAT5 pump glutamate from the extracellular space together with three $Na^+$ and one $H^+$ in the exchange of one $K^+$ upon synaptic release.

EAAT1/GLAST is mainly expressed in Bergmann glial cells within the cerebellum and to a lesser extent in glial cells in the hippocampus, cerebral cortex and thalamus (Chaudhry et al., 1995; Torres and Amara, 2007; Tzingounis and Wadiche, 2007). In developing and adult brain EAAT1/GLAST is also expressed in radial glial cells, in which it plays a role in controlling neuronal migration (Brunne et al., 2010; Mori et al., 2006). For EAAT1/GLAST the anion current component is about one-third of the total transporter current (Wadiche et al., 1995).

EAAT2/GLT-1 is predominantly localized on cerebral astrocytes (Lehre and Danbolt, 1998). Neuronal isoform EAAT3/EAAC1 is ubiquitously expressed in the brain. Both EAAT2/GLT-1 and EAAT3/EAAC1 display low anion conductances in comparison with other EAAT isoforms (Danbolt, 2001; Wadiche et al., 1995).

EAAT4 and EAAT5 are expressed in cerebellar Purkinje cells and bipolar cells of the retina, respectively (Fairman et al., 1995; Arriza et al., 1997) and are predominantly glutamate-gated anion channels (Yamada et al., 1996; Lee et al., 2013; Melzer et al., 2003; Schneider et al., 2014).

## 3.2 Genetic disorders associated with EAAT1/GLAST

A growing number of monogenic disorders caused by mutations in the Solute Carrier Family 1 Member 3 gene (*SLC1A3*) – the gene encoding EAAT1 – have been identified, highlighting the importance of this glial glutamate transporter in brain development and function. Genetic variations in *SLC1A3* were linked to neurological disorders such as Tourette syndrome (Adamczyk et al., 2011), autism and ADHD (van Amen-Hellebrekers et al., 2016), migraine (Kovermann et al., 2017) and episodic ataxia (Jen et al., 2005; de Vries et al., 2009; Pyle et al., 2015; Choi et al., 2017a; Choi et al., 2017b; Iwama et al., 2017).

Episodic ataxia type 6 (EA6) is characterized by epileptic seizures and long-lasting episodes of ataxia (Jen et al., 2005). The first case of EA6 was reported for a 10-year-old boy, heterozygous for an arginine replacement of a highly conserved proline residue in transmembrane domain 5 of EAAT1 (P290R). Throughout his childhood, the patient suffered from ataxia, severe headache, epilepsy and episodes of hemiplegia, lasting for at least twice the duration of those in patients with other types of EA. During his first episode at age 6, EEG revealed subclinical seizure activity, and a magnetic resonance imaging showed mild cerebellar atrophy. Six months later, the second episode of hemiparesis was accompanied by brain swelling and epileptiform discharges. Bifrontal and bioccipital epileptiform activity were also detected by EEG at the last follow-up at age 10 (Jen et al., 2005). Since then EA6 has always been associated with missense mutations in the *SLC1A3* gene (de Vries et al., 2009; Pyle et al., 2015; Choi et al., 2017a; Choi et al., 2017b; Iwama et al., 2017).

## 3.3 Altered function of P290R EAAT1/GLAST

The disease-associated mutation P290R in the *SLC1A3* gene was initially assumed only to modify glutamate transport rates, thus affecting extracellular glutamate concentrations and synaptic transmission. However, in heterologous expression systems P290R was shown to reduce both expression levels of EAAT1 and the glutamate transport rate, simultaneously potentiating anion currents by increasing the open probability of the EAAT1 anion channel (Winter et al., 2012; Hotzy et al., 2013).

Homologous P to R substitution in *Drosophila melanogaster* EAAT1 or expression of human P290R EAAT1 in *Drosophila* larvae caused episodic paralysis. Remarkably, overexpression of $K^+$–$Cl^-$ transporter, extruding $Cl^-$ from the cell, also caused the paralysis in *Drosophila* larvae, while coexpression of the $Na^+$–$K^+$–$2Cl^-$ transporter, responsible for $Cl^-$ accumulation, rescued this phenotype. Furthermore, animals in which the gene encoding EAAT1 was knocked out did not have this phenotype (Parinejad et al., 2016).

A constitutive heterozygous mouse model carrying P290R mutation in EAAT1/GLAST (*Slc1a3*$^{P290R/+}$) exhibits severe ataxia and epileptic seizures, similar to the neurological phenotype in the human patient (Kovermann et al., 2020). Knock-out of *SLC1A3* in mice (*Slc1a3*$^{-/-}$) showed that the complete absence of EAAT1/GLAST-mediated glutamate uptake does not result in seizures, and causes only slight ataxia (Watase et al., 1998; Perkins et al., 2016). These observations suggest that the major pathophysiological condition underlying EA6 is not the reduced glutamate transport, but rather a gain-of-function chloride channelopathy of glial cells expressing P290R EAAT1/GLAST.

## 3.4 Cerebellar degeneration in *Slc1a3*$^{P290R/+}$ mice

We have shown that apoptosis of mutant Bergmann glial cells is the first stage of cerebellar degeneration in *Slc1a3*$^{P290R/+}$ mice eventually resulting in ataxia (Kovermann et al., 2020). Electrophysiological recordings of glutamate-induced anion currents revealed a significantly increased P290R EAAT1/GLAST-mediated $Cl^-$ efflux from Bergmann glial cells, consequently, these cells exhibit reduced intracellular $Cl^-$ concentration ($[Cl^-]_{int}$), that may cause shrinkage-induced apoptosis. Prominent degeneration of Bergmann glial cells was observed in the second postnatal week and spontaneous spiking of the Purkinje neurons of *Slc1a3*$^{P290R/+}$ mice was affected at ~P40, likely resulting in cortical microcircuit dysfunction and cerebellar incoordination. Moreover, in aged *Slc1a3*$^{P290R/+}$ mice we observed a decrease in the overall cerebellar volume. These observations highlight a dramatic impact of the comparably low EAAT1/GLAST anion conductance on glial $Cl^-$ homeostasis.

In epileptic patients, the cerebellar volume is known to correlate with the total number and frequency of generalized tonic-clonic seizures. However, the cerebellar atrophy in these patients was not a predisposing factor for epilepsy, but rather aftermath of epileptic seizures (Hagemann et al., 2002). The cerebellum can affect the epileptic activity arising from other brain regions: cerebellar dysfunction has been shown to facilitate seizure activity in the cerebral cortex (Krook-Magnuson et al., 2014; Dow et al., 1962; Hutton et al., 1972) and cerebellar targeted optogenetic intervention was reported to decrease hippocampal seizure duration (Krook-Magnuson et al., 2014). To date, the seizures arising from the cerebellum have been only reported in patients with tumorous cerebellar lesions like ganglioglioma (Martins et al., 2016) ganglioneurocytoma (Dagcinar et al., 2007), astrocytoma (Strazzer et al., 2006) and hamartoma (Gupta et al., 2003). Thus we concluded that epilepsy in *Slc1a3*$^{P290R/+}$ mice may imply the involvement of some other brain regions.

Recently, quantitative receptor radiography (see chapter 4.6 for method description) was performed in *Slc1a3*$^{P290R/+}$ mice to reveal the brain regions with augmented receptor densities for different neurotransmitters. The densities of α-amino-3-hydroxy-5-methylisoxazole-4-propionic acid (AMPA) ionotropic glutamate receptors were significantly higher in almost all brain regions of

*Slc1a3*$^{P290R/+}$ mice, except for the cerebellum (Fig 3.2, provided by Jennifer Cremer and Sabrina Buller). The most prominent (~30 %) elevation was observed in the hippocampus, implicating its contribution to the pathophysiology of EA6 (unpublished data).

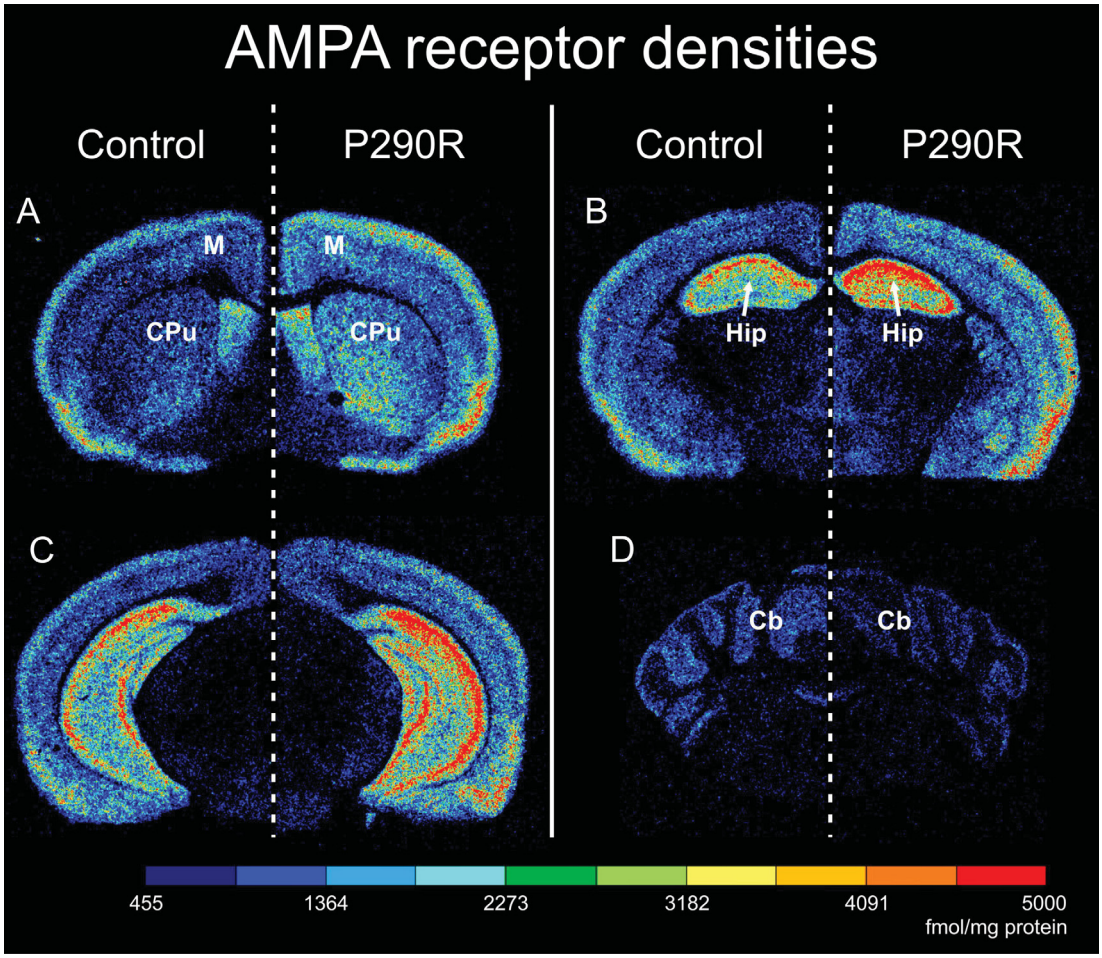


Figure 3.2 (provided by Jennifer Cremer and Sabrina Buller): **AMPA receptor densities in the brain of WT (Control) and *Slc1a3*$^{P290R/+}$ (P290R) mice.** Contrast-enhanced color-coded images showing receptor density differences in cutting plane which includes A: caudate putamen/striatum (Cpu) and motor cortex (M); B: hippocampus (Hip); C: visual cortex and the substantia nigra D: cerebellum (Cb). The assigned color scales with eleven colors represent equally spaced density ranges in fmol/mg protein.

## 3.5 Morphology and signaling circuits of the hippocampus

The hippocampus is part of the temporal lobe and consists of the Cornu Ammonis areas (CA1-3) and the dentate gyrus (DG). The principal neuron types in the hippocampus are the pyramidal cells and the granule cells, residing in the CA and DG respectively.

The DG receives an excitatory input mostly from perforant path fibers of the entorhinal cortex and to a lesser extent from the hilar mossy cells (Blackstad, 1958; Amaral and Winter, 1995). Axons of the granule cells, called mossy fibers, relay signals to the pyramidal cells in the CA3 area. The axons of CA3 pyramidal cells divide into two branches: one branch forms the commissural fibers that project to the contralateral hippocampus, i.e. to another brain hemisphere; the other branch – Schaffer collaterals – projects to the CA1 area and also receives direct input from the perforant path. Lastly, from the CA1 pyramidal cells, the signal goes back through the entorhinal cortex into the re-entrant loop, which can promote feed-forward propagation, making the hippocampal network prone to runaway excitation (Lu et al., 2016). The DG exhibits specialized properties to prevent excitatory inputs from escaping control and triggerring seizures (Heinemann et al., 1992; Lothman et al., 1992).

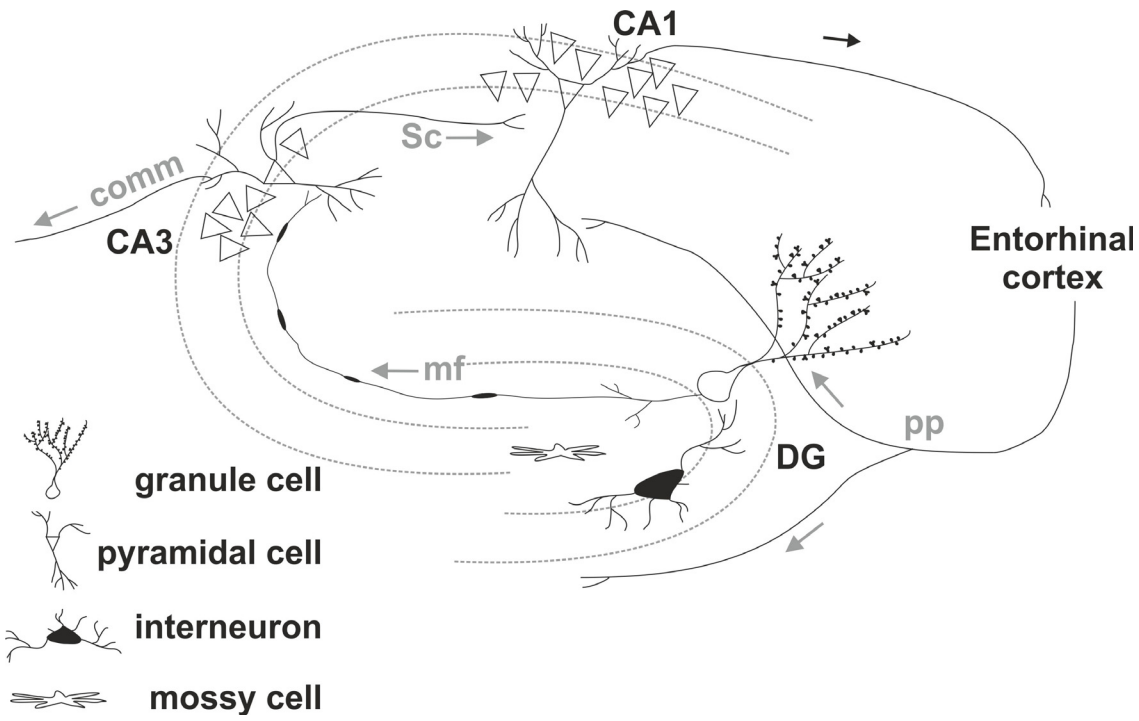


Figure 3.3: **Functional anatomy of the hippocampus.** A trisynaptic loop with a C-shaped organization representing hippocampal circuitry. The major input to the hippocampus – the perforant path (pp) contacts granule cells in the Dentate Gyrus (DG) and pyramidal cells of the CA1 area. Mossy fibers (mf), – axons of granule cells, excite inhibitory interneurons as well as CA3 pyramidal cells, which are connected to contralateral CA3 pyramidal cells through commissural fibers (comm). From CA3 pyramidal cells signals also propagate through Schaffer Collaterals (Sc) to the CA1 area. Lastly, CA1 axons are directly and indirectly connected to the entorhinal cortex, thereby completing the hippocampal trisynaptic circuit.

GABAergic synapses act as the major source of inhibition in the DG (Amaral et al., 2007; Coulter and Carlson, 2007). Besides granule cells, perforant path fibers also innervate GABAergic interneurons (Witter, 2007), that tightly control the activity of granule cells by activating ionotropic $GABA_A$ receptors. Granule cells exhibit $GABA_A$ receptors, located either in the postsynaptic membrane, where they mediate fast phasic neuronal inhibition or at extrasynaptic sites, where they respond to ambient extracellular GABA levels (Semyanov et al., 2003; Lindquist and Birnir, 2006; Farrant and Kaila, 2007; Glykys and Mody, 2007; Martin et al., 2009) and produce long-term tonic inhibition (Coulter and Carlson, 2007; Nusser and Mody, 2002; Stell et al., 2003). The GABA receptor localization within a neuron is determined by its subunit composition (Pirker et

al., 2000): synaptic $GABA_A$ receptors have a prevalent stoichiometry of two α two β and one γ subunits, whereas the expression of a δ instead of a γ subunit results in receptor location outside the synapse and a higher affinity for GABA. Even small changes in tonic current are known to have profound effects on neuronal excitability (Hamann et al., 2002; Mitchell and Silver, 2003; Chadderton et al., 2004), whereas mutations in genes encoding the δ subunit result in epilepsy in mice (Maguire et al., 2005; Peng et al., 2004; Spigelman et al., 2002; Zhang et al., 2007) and humans (Dibbens et al., 2004; Feng et al., 2006; Eugène et al., 2007; Mulley et al., 2005). Thus, altered tonic inhibition of granule cells may represent an initial stage for seizure generation.

## 3.6 EAAT1/GLAST function in the hippocampus

Astrogliopathies in the hippocampus play a critical role in pro-epileptogenic mechanisms in experimental models (Bedner et al., 2015; Kielbinski et al., 2016; Pekny et al., 2016). EAAT1/GLAST makes up approximately 20 % of all cell-surface glutamate transporters in the adult rodent hippocampus (Holmseth et al., 2012), where it is expressed by a specific subpopulation of glial cells, called neural progenitor cells (NPCs) (Brunne et al., 2010; Jungblut et al., 2012; Mori et al., 2006), and by astrocytes (Schreiner et al., 2013).

NPCs are stem cells: their role is to generate new functional granule cells throughout the life of mammals. The first evidence for adult hippocampal neurogenesis was observed in rodents (Altman, 1962) and was subsequently shown to be also present in humans and non-human primates (Kempermann et al., 1997; Kuhn et al., 1996; Eriksson et al., 1998; Roy et al., 2000). While EAAT1/GLAST serves as a marker for the hippocampal NPCs (Jungblut et al., 2012) and an inducible mouse line for GLAST (Glast-$CreER^{T2}$) is widely used for NPCs lineage studies (Mori et al., 2006; DeCarolis et al., 2013), the *in vivo* function of EAAT1/GLAST in NPCs remains still unknown and requires to be investigated.

NPCs generate proliferative precursors, which give rise to neuroblasts and then immature granule cells (Fig. 3.4). Adult-generated granule cells migrate from the subgranular zone to the granule cell layer of the DG, where they integrate into the existing circuitry and participate in normal hippocampal function. It was

suggested that EAAT1/GLAST may regulate NPCs proliferation during development and also affect induced proliferation after injury in a calcium- and metabotropic glutamate receptor (mGluR)-dependent manner (Gilley and Kernie, 2011).

Both NPCs and newborn granule cells do not have synaptic contacts (Moss et al., 2016) and utilize alternative nonsynaptic signaling mechanisms to control their proliferation and migration. One of these mechanisms facilitating cell migration is an activation of ionotropic glutamate receptors, namely N-methyl-D-aspartate (NMDA) receptors. Glutamate uptake via EAAT1/GLAST in NPCs was therefore suggested to modify NMDA-dependent neuronal cell migration by regulating extracellular glutamate levels (Sutherland et al., 1996; Shibata et al., 1997).

Another signaling mechanism modulating NPCs proliferation is achieved by the action of Gamma-Aminobutyric acid (GABA), a major inhibitory neurotransmitter in the central nervous system (Tozuka et al., 2005; Ge et al., 2006; Jagasia et al., 2009; Sun et al., 2009; Duveau et al., 2011). Upon activation, $GABA_A$ receptors selectively conduct $Cl^-$, hyperpolarizing the mature neurons. However, in NPCs and immature neurons, it usually elicits the opposite effect, leading to $Cl^-$ efflux from the cell due to high $[Cl^-]_{int}$ (LoTurco et al., 1995; Owens et al., 1996; Ben-Ari, 2002). Recent studies suggest that the anion channels associated with EAAT1/GLAST are involved in the regulation of glial $[Cl^-]_{int}$ (Untiet et al., 2017). $Cl^-$ transport might also directly affect neuronal proliferation by controlling the cellular volume of dividing cells (Russell, 2000; Sun, 2012). Taken together, these findings suggest a possible role of EAAT1/GLAST-mediated $Cl^-$ conductance in NPCs signaling.

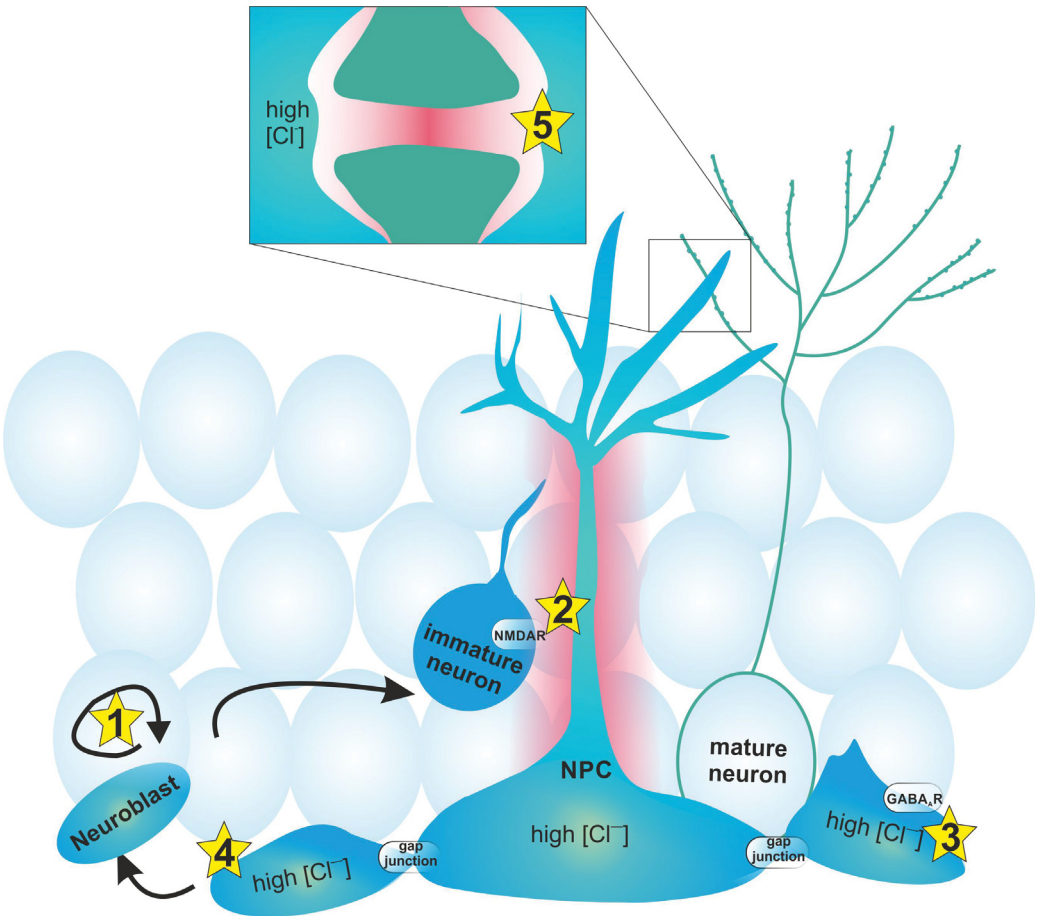


Figure 3.4: **EAAT1/GLAST functions in hippocampal NPCs.** The neurogenic niche of the hippocampus hosts NPCs with radial morphology, neuroblasts, immature and mature granule cells. Possible functions of EAAT1/GLAST highlighted with stars: (1) regulation of the NPCs proliferation in a calcium- and metabotropic glutamate receptor (mGluR)-dependent manner. (2) Control of the extracellular glutamate levels along the radial process, regulating the migration of the immature granule cells via nonsynaptic NMDA receptor activation. (3) Control of the $[Cl^-]_{int}$, enabling depolarizing action of GABA and (4) volume regulation for cell division. (5) Glutamate uptake within the tripartite synapse, formed by NPCs process, dendrite of granule cell and afferent glutamatergic axon.

Supporting this hypothesis, NPCs of *Slc1a3*$^{P290R/+}$ mice exhibit slightly lower $Cl^-$ concentrations (Fig. 3.5, provided by Miriam Engels), as revealed by fluorescence lifetime imaging microscopy (see chapter 4.7 for method description). This demonstrates that EAAT1/GLAST increased $Cl^-$ conductance may not only affect cerebellar Bergmann glial cells, but also hippocampal NPCs and indicates the DG as a possible epileptogenic region in *Slc1a3*$^{P290R/+}$ hippocampus.

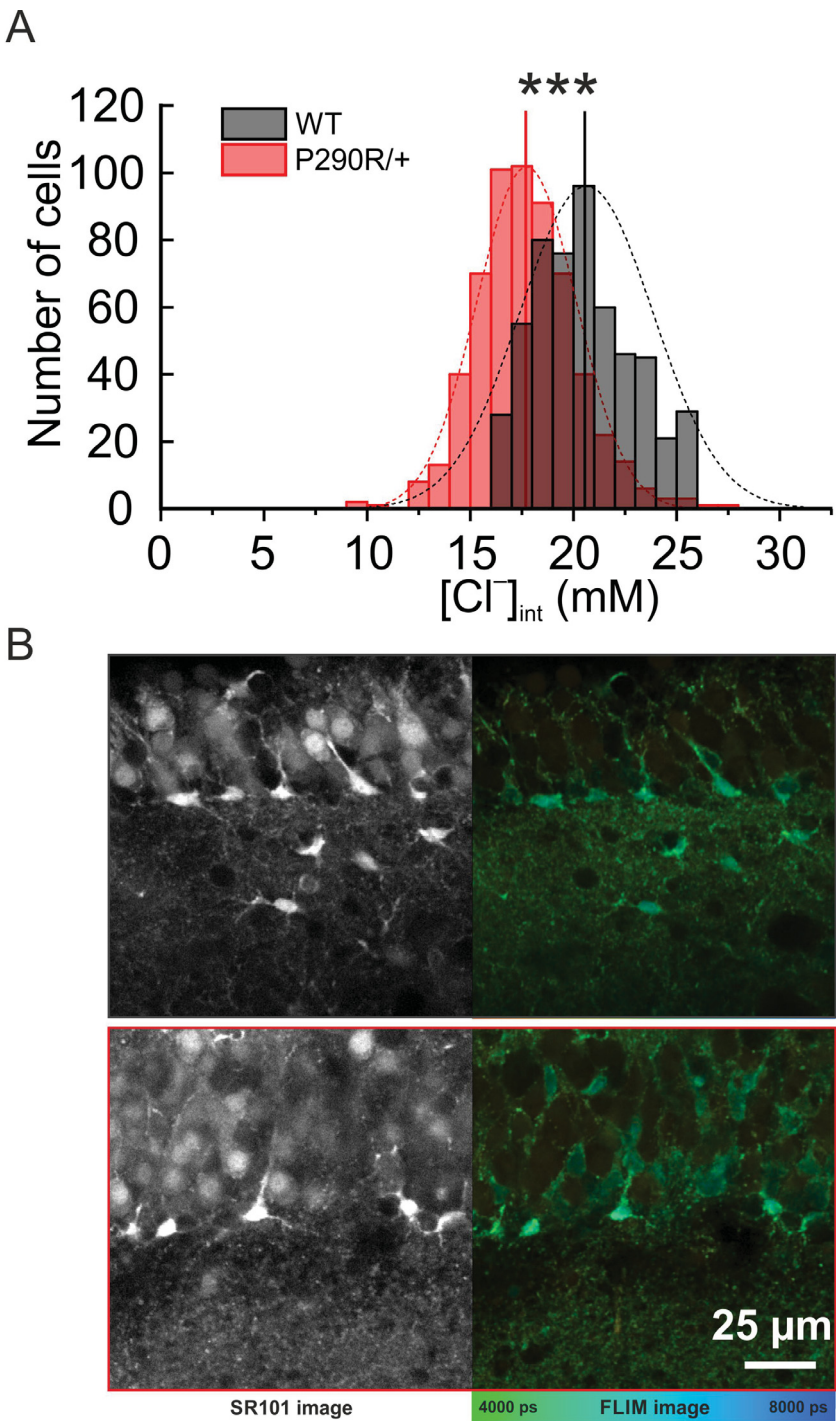


Figure 3.5 (provided by Miriam Engels): **Fluorescence lifetime imaging microscopy in hippocampal NPCs loaded with the $Cl^-$ sensitive dye MQAE.** A: Histograms, representing the $[Cl^-]_{int}$ in WT and *Slc1a3*$^{P290R/+}$ NPCs. The mean $[Cl^-]_{int}$ ± SE is 20.61 ± 0.75 mM and 17.71 ± 0.5 mM in WT and *Slc1a3*$^{P290R/+}$ mice respectively. B: Two-photon images of acute hippocampal slices loaded with SR101 (left) and MQAE (right) in WT (top) and *Slc1a3*$^{P290R/+}$mice (bottom). The average fluorescence lifetime was calculated and color-coded for every single pixel.

The DG serves as a gateway that controls the spread of seizures through the hippocampal network (Behr et al., 1998). Within the DG NPCs share the ensheathing of synapses and vasculature with astrocytes and directly adhere to the adjacent astrocytic processes (Moss et al., 2016). Moreover, NPCs are connected via gap junctions, allowing the intercellular exchange of ions and signaling molecules (Kunze et al., 2009). As NPCs represent a specific cluster of uniquely receptive glial cells, extensively interacting with neurons, glial cells, and vasculature of the DG, the role of EAAT1/GLAST in the DG of epileptic *Slc1a3*$^{P290R/+}$ mice becomes of particular interest.

This work aims to investigate the pathophysiological mechanisms causing epilepsy in *Slc1a3*$^{P290R/+}$ mice. Different attributes of the excitation/inhibition imbalance underlying epileptiform discharges in mutant animals were characterized. For the first time, the role of EAAT1/GLAST anion channel was addressed in hippocampal NPCs and a possible connection of increased EAAT1/GLAST anion channel conductance in NPCs with excessive excitation of hippocampal neurons was suggested.

# 4 Materials & Methods

## 4.1 Animals

### 4.1.1 Mice maintenance

Mice were housed under standard conditions in the animal facility of the Forschungszentrum Jülich GmbH (FZJ) according to institutional guidelines under a 12 h light-dark cycle with food and water provided *ad libitum*. All experiments were approved and in compliance with the German Law for Protection of Animals, and the Landesamt für Natur, Umwelt und Verbraucherschutz (LANUV) of North-Rhine Westphalia (reference 36 nos 84–02.04.2014.A334 and 84–02.04.2014.A335). The health status of mutant mice was systematically monitored and scored using table 4.1. Mice were treated in strict accordance with the defined stop criteria, all efforts were made to minimize animal suffering and reduce the number of animals used.

Table 4.1: **Score sheet and stop criteria for breeding and animal experiments for mouse lines *Slc1a3*$^{P290R/+}$ and *Slc1a3*$^{-/-}$**

| Observation | Score |
|---|---|
| 1. Bodyweight: | |
| correlates with the mean body weight of particular age | 0 |
| decrease: ≤ 5 % of mean body weight of particular age | 1 |
| decrease: 5 – 10 % of mean body weight of particular age | 2 |
| decrease: 11 – 20 % of mean body weight of particular age | 3 |
| decrease: >20 % of mean body weight of particular age | 4 |
| 2. General condition: | |
| smooth and glossy fur; clean orifices of the body, clear, glossy eyes | 0 |
| defects in fur (overwhelming or reduced grooming) | 1 |
| unordered and or dead fur, impure orifices of the body | 2 |
| dead/impure fur, clotted orifices of the body, dreary eyes | 3 |
| clear breath sounds, animal feel cold, seizures | 4 |

| | |
|---|---|
| 3. Spontaneous behavior | |
| Normal behavior (animal react on blowing/touches), normal social contacts | 0 |
| slight problems in motor coordination, temporary tremor, normal social contacts | 1 |
| limited motor coordination, clear, rare rearing and climbing | 2 |
| Isolation, lethargy and curved posture | 3 |
| Isolation, lethargy and curved posture with frequent seizures (>1/8h) or longer than 2 minutes | 4 |
| 4. Symptomatic (episodic ataxia) | |
| no symptoms | 0 |
| slight ataxia, food and water is reached easily, temporary tremor | 1 |
| clear ataxia, tremor, and short focal seizures, w/o loss of righting reflex, frequency <1/8h, food and water is consumed | 2 |
| heavy ataxia, short focal seizures, w/o loss of righting reflex (<2/8h), with relaxing phase | 3 |
| heavy ataxia with frequent focal seizures and loss of righting reflex for >2 minutes or frequency of seizures >1/day | 4 |

### 4.1.2 EAAT1/GLAST knock-in (*Slc1a3*$^{P290R/+}$) mouse model

The knock-in *Slc1a3tm1P290RCfa* (*Slc1a3*$^{P290R/+}$) mice were generated by site-directed mutagenesis using a mutant *Slc1a3* allele located on chromosome 15 (at 3.82 cM) and encoding a P290R substitution in transmembrane domain 5. Briefly, a 13,851 bp XbaI fragment covering exons 4–8 of the *Slc1a3* locus was subcloned from BAC bMQ-99B1 (Polygene Transgenetics) into the pLit28 cloning vector. The P290R sequence (agg to gcg) was inserted via polymerase chain reaction (PCR) synthesis into the end of exon 7. A silent mutation 6 bp upstream of P290 was included to insert a unique BamHI site for PCR-coupled restriction fragment length polymorphism or Southern blot analysis to confirm the presence of the P290R mutation in embryonic stem cells (ES) and mice. An FRT-flanked neomycin resistance cassette was inserted into a MluI restriction

site 154 bp upstream of exon 7 for selecting mutated ES cells (Fig. 4.1). The targeting vector was then linearized and electroporated into ES cells (107 cells); Cells that had undergone homologous recombination were selected using G418-supplemented medium (0.2 mg/ml) and confirmed by PCR and Southern blot hybridization.

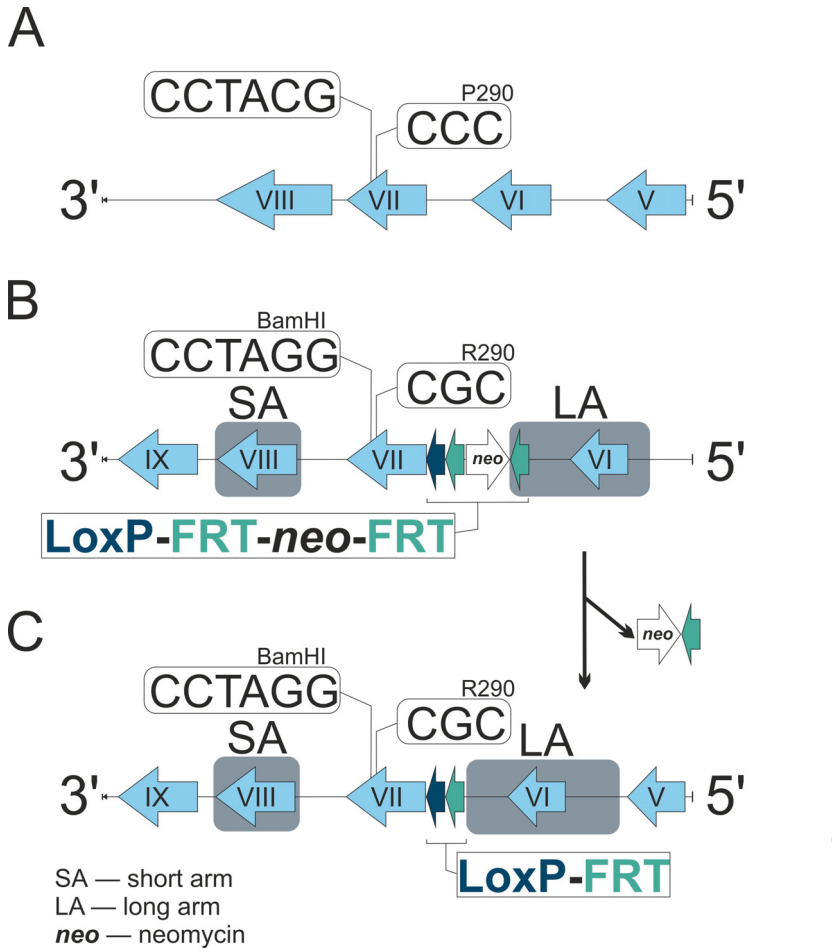


Figure 4.1: **Targeting strategy and verification of *Slc1a3* transgene insertion.** Schematic diagram showing the location of the P290R mutation in EAAT1/GLAST. A: target codons for the WT *Slc1a3*-targeting construct used for homologous recombination. B: recombinase-mediated nucleotide exchange inserts the mutation and an FRT-flanked neomycin cassette (for selection) into exon VII (SA, short arm; LA, long arm; neo, neomycin). C: the mutated *Slc1a3* gene after Flp-mediated excision of the neomycin cassette.

Correctly homologous recombined ES cell clones were identified and injected into a blastocysts from C57BL/6 (Charles River) mice to produce germline chimeric animals in CD-1 foster mice (Polygene Transgenetics), which were crossbred with FLP-deleter mice (B6;SJLTg(ACTFLPe)9205Dym/J; Janvier Labs) to excise the neomycin cassette. BamHI restriction of the heterozygous P290R mutant verified P290R 37 substitution in C57BL/6N mice. Knock-in mice were backcrossed into the more robust mouse strain 129/SvJ (Taconic Biosciences GmbH) for 10 generations. PCR genotyping was performed with primers A219.5 – AAGAGGATCCCCAGGCGCGCATACCTGCGGC and A219.6 CAGGCTGTGGCATGGACAAC (Polygene Transgenetics). The sizes of amplified PCR products of the different genotypes using the corresponding primers were: 478 bp (EAAT1/GLAST WT), 739 bp (*Slc1a3*$^{P290R/+}$).

### 4.1.3 EAAT1/GLAST knock-out (*Slc1a3*$^{-/-}$) mouse model

Heterozygous EAAT1/GLAST knock-out (*Slc1a3*$^{-/-}$) mice were obtained from Dr. Niels Danbolt (Institute of Basic Medical Science, University of Oslo) and generated as described before (Watase et al., 1998) in a C57BL/6N (B6.129P2) background. Heterozygous animals were bred because of poor nesting behavior of homozygous knock-out animals. PCR genotyping was performed with primers (A/B/C/D)
GLAST-KO-A – AAGTGCCTATCCAGTCCAACGA,
GLAST-KO-B – AAGAACTCTCTCAGCGCTTGCC,
GLAST-KO-C – AATGGAAGGATTGGAGCTACGG and
GLAST-KO-D – TTCCAGTTGAAGGCTCCTGTGG (Eurofins Genomics). The sizes of amplified PCR products of the different genotypes using the corresponding primers were 214 bp (EAAT1/GLAST WT) and 383 bp (*Slc1a3*$^{-/-}$).

### 4.1.4 Genotyping

DNA was isolated from tail biopsies. Genotypes were tested with the KAPA Mouse Genotyping hot start kit (Peqlab) and primers A219.5/6 or GLAST-KO A/B/C/D. Amplified PCR products were analyzed on a 1.5 % agarose gel, 25 min, 80 V, 200 mA, and their size was compared to a 100 bp gene ruler (Thermo Scientific).

## 4.2 Electrophysiology

### 4.2.1 Slice preparation

Acute brain slices were prepared as described earlier (Edwards et al., 1989). Mice were anesthetized with isoflurane and decapitated. Brains were rapidly removed from the skull and placed in oxygenated ice-cold Preparation-Ringer's solution. Parasagittal 250 µm-thick slices were cut with a vibrating blade microtome (HM650V, Thermo Scientific, frequency 60, amplitude 1, drive 10). Slices containing hippocampi were transferred to a gaze slice holder basket arranged in oxygenated Preparation-Ringer's solution at 37°C. After 30 min, slices were left to equilibrate for at least 90 min in oxygenated Normal-Ringer's solution at room temperature (RT, 20 – 22°C), where they were stored until usage. During all experiments, solutions were constantly oxygenated with carbogen (5 % $CO_2$ in $O_2$). Single slices were transferred to a recording chamber, perfused continuously with oxygenated Normal-Ringer's at RT. Cells were visualized by infrared gradient contrast video microscopy (Andor Neo sCMOS, Oxford Instruments) using Solis software and a 40x water-immersion objective (Olympus 40x/0.80 w).

### 4.2.2 Whole-cell voltage-clamp recordings

Recordings from individual granule and pyramidal cells were made using pipettes (resistance, 6–8 MΩ) prepared from borosilicate glass capillaries (Harvard Apparatus) with a micropipette puller (Sutter Instrument) at RT. An EPC10 USB patch-clamp amplifier (HEKA Elektronik) in voltage-clamp mode at 0 mV for 1 to 10 min and sampling at 10 kHz (Patch Master Software, HEKA Elektronik) was used for electrophysiological recordings. Pipettes were filled with CsCl-based solution supplemented with QX-314 (Tocris Bioscience) to block the $GABA_B$ receptor currents and to prevent the generation of $Na^+$-dependent action potentials. All whole-cell recordings were made under continuous perfusion with Normal Ringer's solution at RT supplemented with 1 µM tetrodotoxin (Tocris Bioscience) and 50 µM D-AP5 (Tocris Bioscience) in order to block $Na^+$ channels and NMDA receptor currents, respectively. The cells were generally held at a membrane potential of −70 mV and the liquid junction potential was not corrected. AMPA receptor-mediated mEPSCs were

recorded in the presence of 1 µM picrotoxin (PTX) to block $GABA_A$ receptors. Recordings of GABAergic miniature inhibitory postsynaptic currents (mIPSCs) and tonic currents were taken in the presence of 10 µM cyanquixaline (CNQX) to avoid AMPA receptor-mediated signals. To isolate tonic current 50 µM PTX was added in the bath solution. 30 s epochs before PTX application (baseline) and after 3 min of continuous perfusion with a blocker were compared by histograms of current values. Data was analyzed off-line using Clampfit event analysis functions (Molecular Devices).

## 4.3 Immunohistochemistry

### 4.3.1 Preparation of cryo slices and paraffin-embedded slices

The brains were prepared as described in the chapter 4.2.1 and fixed with 4 % paraformaldehyde (PFA, $[CH_2O]_n$) in PB (in mM: 81 $NaH_2PO_4 \cdot 2H_2O$, 9 $Na_2HPO_4H_2O$, pH 7.4) for 30 min at 4°C. Then the brains were washed in PB (30 min, RT) and incubated in PB supplemented with 10 % sucrose for 1 h at RT and 30 % sucrose for 12 h at 4°C).

Hemispheres were embedded in NEG50 (Thermo Scientific) and cut into 14 µm-thick sagittal slices using an HM560 cryotome (MICROM).

For VGLUT1 and VGLUT2 immunostaining, brains were stored in PFA for 5 days at 4°C for the fixation. After dehydration in a graded ethanol series (50 %, 70 %, 90 %, 100 % EtOH) brains were embedded in paraffin and 5 µm-thick sagittal sections were cut. Before immunostaining, endogenous peroxidases were inactivated by a solution containing (in mM) 21 $C_6H_8O_7$, 6 $Na_2HPO_4$ and 15 % (v/v) $H_2O_2$ for 15 min at RT. Epitopes were unmasked using a solution containing 2M Tris and 63 EDTA mM (pH 8.0), at 100°C for 20 min. Sections were blocked overnight at 4°C in 1 % (w/v) bovine serum albumin diluted in PB.

Cryo and paraffin sections were incubated overnight at 4°C in primary antibodies and afterward for 45 min at RT in cyanine dye-conjugated secondary antibodies. Both primary and secondary antibodies were diluted in 5 % ChemiBLOCKER (Merck–Millipore) in PB, containing 1 % Triton-X100 and 0.05 % $NaN_3$. A list of all used antibodies is provided in Table 4.2.

Table 4.2: **Antibodies used for immunohistochemical protein detection**

| Target | Host | RRID | Dilution | Supplier |
|---|---|---|---|---|
| 1st antibodies | | | | |
| BLBP | *rabbit* | AB_10000325 | 1:200 | Merck Millipore |
| GFAP | *chicken* | AB_1556315 | 1:2000 | Novus Biologicals |
| GLAST | *mouse* | AB_10829302 | 1:500 | Milteniy Biotec |
| VGLUT1 | *rabbit* | AB_887875 | 1:100 | Synaptic systems |
| VGLUT2 | *ginea pig* | AB_2301731 | 1:10000 | Merck Millipore |
| 2nd antibodies | | | | |
| *chicken* Immunoglobulin G (Cy2 conjugate) | *donkey* | AB_2340370 | 1:200 | Jackson Immuno Research Labs |
| *guinea pig* Immunoglobulin G (Cy3 conjugate) | *donkey* | AB_2340460 | 1:800 | Jackson Immuno Research Labs |
| *rabbit* Immunoglobulin G (Cy3 conjugate) | *donkey* | AB_2340612 | 1:500 | Jackson Immuno Research Labs |
| *mouse* Immunoglobulin G (Cy5 conjugate) | *donkey* | AB_2340813 | 1:400 | Jackson Immuno Research Labs |

### 4.3.2 Quantification of VGLUT1 and VGLUT2 punctae

Slides were coverslipped using Fluoromount Aqueous Mounting medium (Polysciences) and signals were visualized under a confocal microscope (Leica TCS SPS II) with oil immersion objectives (HCX PL APO CS 20.0x0.70 and 63.0x1.40). Punctae densities were quantified by counting VGLUT1-positive and VGLUT2-positive signals in randomly selected areas of different sizes within single confocal planes using the software ImageJ (National Institutes of Health). VGLUT1 signals were addressed in the CA3 region, where mossy fibers terminate onto pyramidal cells, whereas VGLUT2 was counted within the granule cell layer of DG. Punctae densities are given as boutons per 100 $\mu m^2$.

## 4.4 Determination of protein expression levels

To quantify relative protein expression levels, western blots were performed from hippocampal lysates.

### 4.4.1 Protein extraction and BCA assay

For protein extraction, at least 3 animals per genotype and age group were tested. The brains were prepared as described in the chapter 4.2.1. The whole hippocampi were separated from the brain and frozen in liquid nitrogen.
Hippocampi were homogenized using a homogenizer containing ice-cold lysis buffer at 4°C. The homogenate was centrifuged at 55000 RCF for 45 min, at 4° C. The supernatant (cytosolic fraction) was frozen, and the pellet containing the total crude membrane was solubilized with solubilizing buffer.
The protein concentration was determined with a BCA assay (high range) according to the factory recommendations. Extinctions were measured on a NanoDrop 2000 (Thermo Scientific, Absorption at 280 nm).

### 4.4.2 SDS-PAGE

Western blots were performed using the BIOMETRA™ Multigel-Long gel system with a 12 % separation gel. The 5 µg of membrane protein were loaded onto the gel. As a molecular marker 2 µl of the color marker PageRuler™ Plus Prestained Protein Ladder (Thermo Scientific) was used. The gel ran for 120 min at 200 V at RT.

### 4.4.3 Western blot

Two sheets of blotting paper saturated with Anode transfer buffer I and one sheet saturated with Anode transfer buffer II were superimposed over the anode plate of the Semi-dry blotter (V20-SDB Scie-Plas, Harvard Apparatus), followed by the membrane, the gel and a further 3 sheets of blotting paper saturated with cathode transfer buffer. The cathode plate was then placed over the blotting sandwich and the current applied at 1 mA per $cm^2$ for 25 min.

### 4.4.4 Immunodetection of proteins

The membrane was blocked for 60 min with 3 % (w/v) BSA (PBS-T) at RT with gentle shaking. Then the membrane was incubated with the primary antibody for 60 min (RT, Table 4.3) and washed three-fold for 10 min with PBS buffer containing 0.05 % Tween-20 (Sigma Aldrich) before the secondary antibody was applied for 45 min at RT. The membrane was washed again three-fold for 10 min with PBS-T buffer containing 0.05 % Tween-20 and one time with PBS alone. Until chemiluminescence imaging, the membrane was kept constantly in PBS.

Table 4.3: **Antibodies used for immunodetection of EAAT1/GLAST, EAAT2/GLT-1, GAT-3, and actin**

| Target | Host | RRID | Dilution | Supplier |
|---|---|---|---|---|
| 1st antibodies | | | | |
| GLAST | *mouse* | AB_10829302 | 1:1000 | Milteniy Biotec |
| GLT-1 | *ginea pig* | AB_90949 | 1:2000 | Merck Millipore |
| GAT-3 | *rabbit* | AB_304437 | 1:500 | Abcam |
| 2nd antibodies | | | | |
| *mouse* Immunoglobulin G (HRP conjugate) | *rabbit* | AB_228415 | 1:25000 | Thermo Scientific |
| *guinea pig* Immunoglobulin G (HRP conjugate) | *rabbit* | AB_10981814 | 1:25000 | Thermo Scientific |
| *rabbit* Immunoglobulin G (HRP conjugate) | *goat* | AB_228333 | 1:25000 | Thermo Scientific |

Table 4.4: **Size and isoelectric point of proteins of interest**

| Protein | Size | Isoelectric point |
|---|---|---|
| GLAST | 58 kDa | 8.52 |
| GLT-1 | 62 kDa | 6.09 |
| GAT-3 | 74 kDa | 6.2 |
| Actin | 42 kDa | 4.8 |

### 4.4.5 Chemiluminescence imaging

Chemiluminescence imaging was performed using the GeneGnome and the software GeneSys (Syngene). The membrane was gently dried and covered with 800 µl SuperSignalTM (Thermo Scientific).

### 4.4.6 Blot analysis

Quantification of western blot band intensities was performed with ImageJ. Profile blots for each captured signal depict the relative density of the respective lanes, with darker and broader signals resulting in higher and wider peaks, respectively. The background signal was subtracted from the final quantification value. The relative expression of EAAT1/GLAST, EAAT2/GLT-1, and GAT-3 was estimated by calculating the ratio between the amount of target protein and the corresponding control band of actin.

## 4.5 Golgi-Cox staining

### 4.5.1 Staining

Golgi-Cox staining was performed as described previously (Zaqout and Kaindl, 2016). After anesthesia with isoflurane mice were decapitated, brains were removed, washed with PBS, and incubated in 20 ml of Golgi-Cox solution for 24 h at RT in the dark. Then, brains were transferred to fresh Golgi-Cox solution and incubated for 10 days. The brains were moved to a tissue-protectant solution and kept for 24 h at 4 °C in the dark. After 24 h, brains were moved into the fresh tissue-protectant solution and incubated for 7 days. 100 µm-thick slices were cut using vibrating blade microtome (HM650V, Thermo Scientific, frequency 60, amplitude 1, drive 7) and placed on slides coated with 3 %

gelatine. The slides were put into cuvettes and dried for 3 days in the dark. The sections were then rinsed twice with bi-distilled water for 5 min each and immersed in 50 % ethanol for 5 min. After incubation in 3:1 $NH_3$ solution (prepared by mixing 200 ml $NH_3$ solution with 100 ml bi-distilled water) for 8 min at RT, the sections were rinsed twice with bi-distilled water each time for 5 min. Afterward the sections were incubated in 5 % $Na_2SO_3$ solution for 10 min at RT in the dark and washed 1 min with bi-distilled water. Dehydration was performed in an ethanol series (50 %, 95 % and 100 % ethanol for 6 min each). After incubating the samples in RotiClear (Carl Roth Gmbh) for 6 min, the sections were mounted in Malinol (Muto Pure Chemicals), coverslipped and left for at least 60 min at RT to dry.

### 4.5.2 Dendritic spine quantification

Brightfield confocal z-stack images with a 0.5 µm interval were acquired using HCX PL APO CS 63.0x1.40 oil immersion objective and a Leica TCS SPS II confocal microscope. A total of 3–11 individual 10 µm dendritic segments were quantified from each hippocampus. Only protrusions with a clearly discernible spine head and neck along the secondary and tertiary dendrites of granule cells and CA1 pyramidal cells were selected for analysis. Spine analysis was performed using the freely available Reconstruct Software version 1.1.0.0 (Fiala, 2005). Using the ‘Draw Z-trace’ tool and scrolling through the different stacks, the three-dimensional length of each protrusion (from the beginning of the spine neck to the tip of the spine head) was measured. Spine width was measured by drawing a straight line across the widest point of each spine head in a single image of the z-series. This data was transferred to LibreOffice Calc, where the spine types were determined based on the ratio of the spine head width to the spine neck length and classified as: filopodia (length > 2 µm), long thin (length > 1 µm), thin (length <1 µm), stubby (length: width ratio approx.: 1:1, no spine neck visible), mushroom (width > 0.6 µm) and branched (if number of heads > 1). Each morphological category was quantified as a percentage of total spines for each segment and averaged for each genotype. The linear spine density was calculated by dividing the total number of counted spines by the length of the sampled dendritic segment. In total 338 spines (DG WT animals) and 425 (DG P290R) spines were categorized.

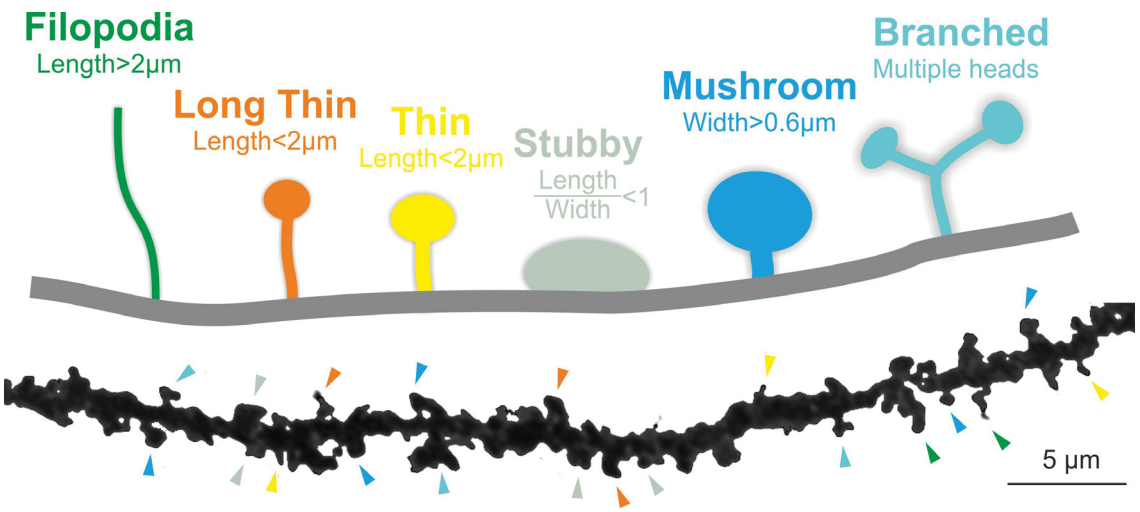


Figure 4.2: **Common dendritic spine types within the hippocampus.** The range of dendritic spines that are common when examining the dendrites of hippocampal neurons. Different spine types are indicated below, on a Golgi-Cox stained granule cell secondary dendritic branch by arrowheads, color-coded to match. Geometric characteristics of spines, shown below each type, are used for the spine analysis method.

## 4.6 Statistical analysis

For all different experimental conditions, statistical analysis was performed by a 2-tailed student's *t*-test, or, if the values were not normally distributed, by using the Mann-Whitney Rank Sum Test. Asterisks indicate the level of significance (***, $p < 0.001$; **, $p < 0.01$; *, $p < 0.05$). A normal distribution of datasets was verified by Shapiro-Wilk tests. All determined values, test results, numbers of cells, slices, and animals used are listed in tables 5.1-5.4.

### 4.6.1 Kaplan-Meier analysis of time to first seizure

Kaplan–Meier survival analysis was performed to estimate the chance to be free of seizures at various time points after birth for male and female *Slc1a3*$^{P290R/+}$ mice. This particular statistical technique was used because of the ability to handle different lengths of follow up caused by censored observations such as killing for the experimental use. The estimator of the survival function $\hat{S}(t)$ is given by:

$$\hat{S}(t) = \prod_{i=0}^{\infty} \frac{n_i - d_i}{n_i}$$

where $n_i$ is the number of mice that have not yet had a seizure or have not been censored at time $t_i$, and $d_i$ is the number of observed events and censored observations at time $t_i$. To compare distributions for males and females, significance was ascertained by the Log-Rank test. A p-value of less than or equal to 0.05 was deemed as statistically significant.

*The current study profited from results of quantitative receptor autoradiography experiments (chapter 4.6), performed by Jennifer Cremer and Sabrina Buller as well as fluorescence lifetime imaging microscopy (chapter 4.7), performed by Miriam Engels.*

## 4.7 Quantitative receptor autoradiography

Quantitative receptor autoradiography was performed according to the previously described protocol (Zilles et al., 2002a, b). Brains from mice at P42-47 were deep-frozen and serially sectioned (10 µm) in the coronal plane. Slices were incubated in solutions containing tritiated ligands (Table 4.5) and exposed against β-sensitive films. The mean densities of glutamatergic, GABAergic and dopaminergic receptors were quantified in different brain regions and visualized via color-coding (Zilles et al., 2002a).

Table 4.5: **Tritiated ligands used for quantitative receptor autoradiography**

| Neurotransmitter | Receptor subtype | Tritiated ligand |
|---|---|---|
| Glutamate | AMPA | [$^3$H]AMPA |
| | kainate | [$^3$H]kainate |
| | NMDA | [$^3$H]MK 801 |
| | mGlu2/3 | [$^3$H]LY 341495 |
| GABA | $GABA_A$ | [$^3$H]muscimol |
| | $GABA_B$ | [$^3$H]CGP 54626 |
| Dopamine | D2/D3 | [$^3$H]fallypride |

Densities of each binding site were analyzed for statistically significant differences between WT and *Slc1a3*$^{P290R/+}$ mice using ANOVAs (repeated measures design, blocking factor: animal, between factor: experimental status, within factor: ROI, response variables: binding site densities). Statistically significant findings ($p<0.05$) were followed by post hoc ANOVAs for each ROI.

## 4.8 Fluorescence lifetime imaging microscopy

Acute 250 µm-thick slices, containing hippocampi, were prepared as described in the chapter 4.2.1 and incubated with sulforhodamine 101 (SR101) and N-[ethoxycarbonylmethyl]-6-methoxy-quinolinium bromide (MQAE) in Normal Ringer's solution for 30 min. NPCs were identified by SR101 staining and their

morphological structure and localization within the subgranular layer of the DG. MQAE is a fluorescent dye, which fluorescence is collisionally quenched by $Cl^-$ ions, resulting in a linear relationship between the inverse fluorescence lifetime and $[Cl^-]_{int}$ (Verkman, 1990). After calibration in NPCs using the 2-ionophore calibration experiments (Untiet et al., 2017), $[Cl^-]_{int}$ for single NPCs soma was calculated from the mean fluorescence lifetime of all pixels within a defined region of interest. $[Cl^-]_{int}$ are given as means ± 95 % CI from repeated experiments.

## 4.9 Buffer

Ringer's solution (10x)

| | |
|---|---|
| 1250 mM | NaCl |
| 25 mM | KCl |
| 12.5 mM | $NaH_2PO_4$ |
| 260 mM | $NaHCO_3$ |

Filtered and stored at 4°C.

Normal Ringer's solution

| | |
|---|---|
| 2 mM | $CaCl_2$ |
| 1 mM | $MgCl_2$ |
| 10 v/v | 10 x Ringer's solution |
| 10 mM | D-glucose |

Preparation Ringer's solution

| | |
|---|---|
| 0.5 mM | $CaCl_2$ |
| 5 mM | $MgCl_2$ |
| 10 v/v | 10 x Ringer's solution |
| 25 mM | D-glucose |

Intracellular solution

| | |
|---|---|
| 130 mM | CsCl |
| 8 mM | NaCl |
| 10 mM | HEPES |
| 2 mM | EGTA |
| 0.2 mM | $MgCl_2$ |
| 4 mM | Mg-ATP |
| 0.3 mM | Li-GTP |
| 1 mM | QX-314 |

295 mOsm, pH adjusted to 7.2 with CsOH.

Separating gel (10 %)

| | |
|---|---|
| 0.375 M | Tris-HCl, pH 8.8 |
| 0.1 % | Sodium dodecyl sulfate (SDS) |
| 10 % | Acrylamide bis solution |
| 0.05 % | Ammonium persulfate (APS) |
| 0.1 % | TEMED |

Stacking gel (5 %)

| | |
|---|---|
| 0.125 M | Tris-HCl, pH 6.8 |
| 0.1 % | SDS |
| 5 % | Acrylamide bis solution |
| 0.05 % | APS |
| 0.1 % | TEMED |

Phosphate buffered saline (PBS)

| | |
|---|---|
| 140 mM | NaCl |
| 2.7 mM | KCl |
| 10 mM | $NaH_2PO_4$ |
| 1.8 mM | $KH_2PO_4$ |

PBS-T buffer

| | |
|---|---|
| 99.95 % | PBS |
| 0.05 % | Tween 20 |

Anode transfer buffer I

| | |
|---|---|
| 0.3 M | Tris pH 10.4 |
| 20 % | Methanol |

Anode transfer buffer II

| | |
|---|---|
| 0.025 M | Tris pH 10.4 |
| 20 % | Methanol |

Kathode transfer buffer

| | |
|---|---|
| 0.025 M | Tris pH 9.4 |
| 0.04 M | Glycin |
| 20 % | Methanol |

SDS sample buffer (4x)

| | |
|---|---|
| 200 mM | Tris-Cl pH 6.8 |
| 8 % | SDS |
| 4 % | β-mercaptoetanol |
| 50 % | Glycerol |
| 0.04 % | Bromophenol blue |

SDS running buffer, pH 8.3

| | |
|---|---|
| 25 mM | Tris |
| 192 mM | Glycine |
| 0.1 % | SDS |

Lysis buffer

| | |
|---|---|
| 2 mM | EDTA |
| 2 µl/ml | Protease inhibitor cocktail |
| 40 µl/ml | COmplete, EDTA-free |

Solubilizing buffer

| | |
|---|---|
| 1 % (w/v) | SDS |
| 10 mM | Sodium phosphate, pH 8.0 |
| 40 µl/ml | COmplete, EDTA-free |

Golgi-Cox solution

| | |
|---|---|
| 1.25g/120ml | $K_2Cr_2O_7$ |
| 1.25g/120ml | $HgCl_2$ |
| 1g/120ml | $K_2CrO_4$ |

The solution was kept at RT for at least 48 h before use to allow the precipitate formation and was used within 1 month.

Tissue-protectant solution

| | |
|---|---|
| 11.5 mM | $NaH_2PO_4$ |
| 38.5 mM | $Na_2HPO_4$ |
| 154 mM | NaCl |
| 33 % (w/v) | Sucrose |
| 1 % (w/v) | Polyvinylpyrrolidone |
| 33 % | Ethylene glycol |

# 5 Results

## 5.1 Generalized epileptic seizures in male and female *Slc1a3*$^{P290R/+}$ mice

Bodyweight and health conditions of WT and *Slc1a3*$^{P290R/+}$ mice were visually checked twice per day starting from P15, and their fitness was scored with respect to general condition, behavioral aspects, and EA6 associated pathology (Table 4.1). Mice with scores ≥4 or that exhibited severe epilepsy were euthanized. The Kaplan-Meier curve shows that male *Slc1a3*$^{P290R/+}$ mice have slightly earlier onset of the seizure period than female mice, with the earliest onset on P24 and P30 respectively. The latest seizure was observed on P54 in male and P68 in female mice. Male *Slc1a3*$^{P290R/+}$ were also slightly more affected by seizures than females (29/23 %, N=139/152, males/females). However, these differences are not statistically significant, thus we conclude that *Slc1a3*$^{P290R/+}$ males and females are similarly affected by epileptic seizures.

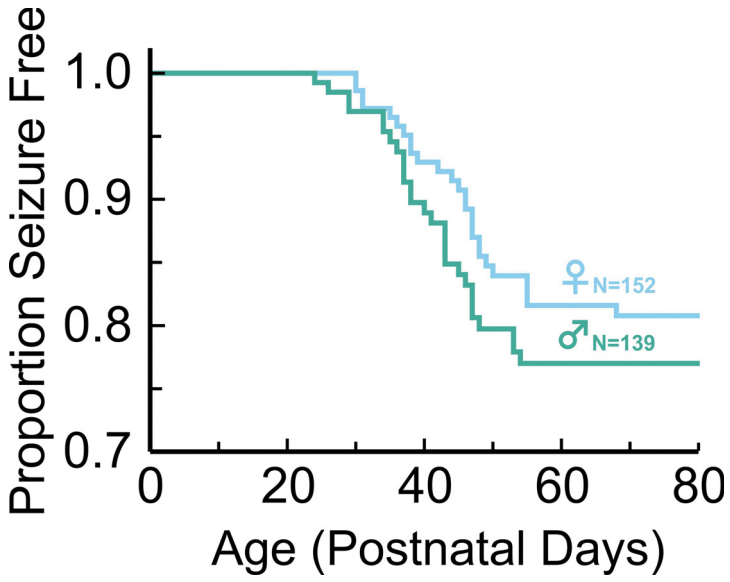


Figure 5.1: **Seizure susceptibility of male and female *Slc1a3*$^{P290R/+}$ mice.** Kaplan–Meier curves showing the proportion of mice that are seizure-free as a function of age. Censored mice (seizure-free at last follow-up) are included in the analysis. Mutant males and females show no significant difference in seizure susceptibility (Log-rank statistic, $p > 0.05$).

## 5.2 Increased AMPA receptor-mediated mEPSC in *Slc1a3*$^{P290R/+}$ hippocampi

Brain regions, in which potentially impaired neurotransmission might be responsible for epilepsy in *Slc1a3*$^{P290R/+}$ mice, were addressed using quantitative autoradiography. Mutant hippocampi revealed increased densities of AMPA receptors (Fig. 3.2). To check if AMPA receptor-mediated excitatory neurotransmission is affected in *Slc1a3*$^{P290R/+}$ mice, whole-cell patch-clamp recordings were carried out in acute hippocampal slices. Action potentials, GABA receptors, and NMDA receptors were blocked by tetrodotoxin, PTX, and AP-5 respectively, to isolate spontaneous AMPA receptor-mediated mEPSCs. Representative traces of AMPA receptor-mediated mEPSCs in WT and *Slc1a3*$^{P290R/+}$ mice are shown in Fig. 5.2. Currents from granule cells and CA1 pyramidal cells were recorded. The amplitude, frequency and decay times of the AMPA receptor-mediated mEPSCs are not different in WT and *Slc1a3*$^{P290R/+}$ hippocampi, before seizure onset (P19-27), so that increased AMPA receptor-mediated neurotransmission cannot be a major reason for epilepsy in *Slc1a3*$^{P290R/+}$ mice. However, amplitudes of the AMPA receptor-mediated mEPSC are significantly increased in granule cells (mean: WT = 3.90 ± 0.15 pA, *Slc1a3*$^{P290R/+}$ = 4.80 ± 0.26 pA), and CA1 pyramidal cells (mean: WT = 3.35 ± 0.16 pA, *Slc1a3*$^{P290R/+}$ = 4.72 ± 0.32 pA) after seizure onset (P41-57), suggesting their contribution to the seizure maintenance in the mutant animals.

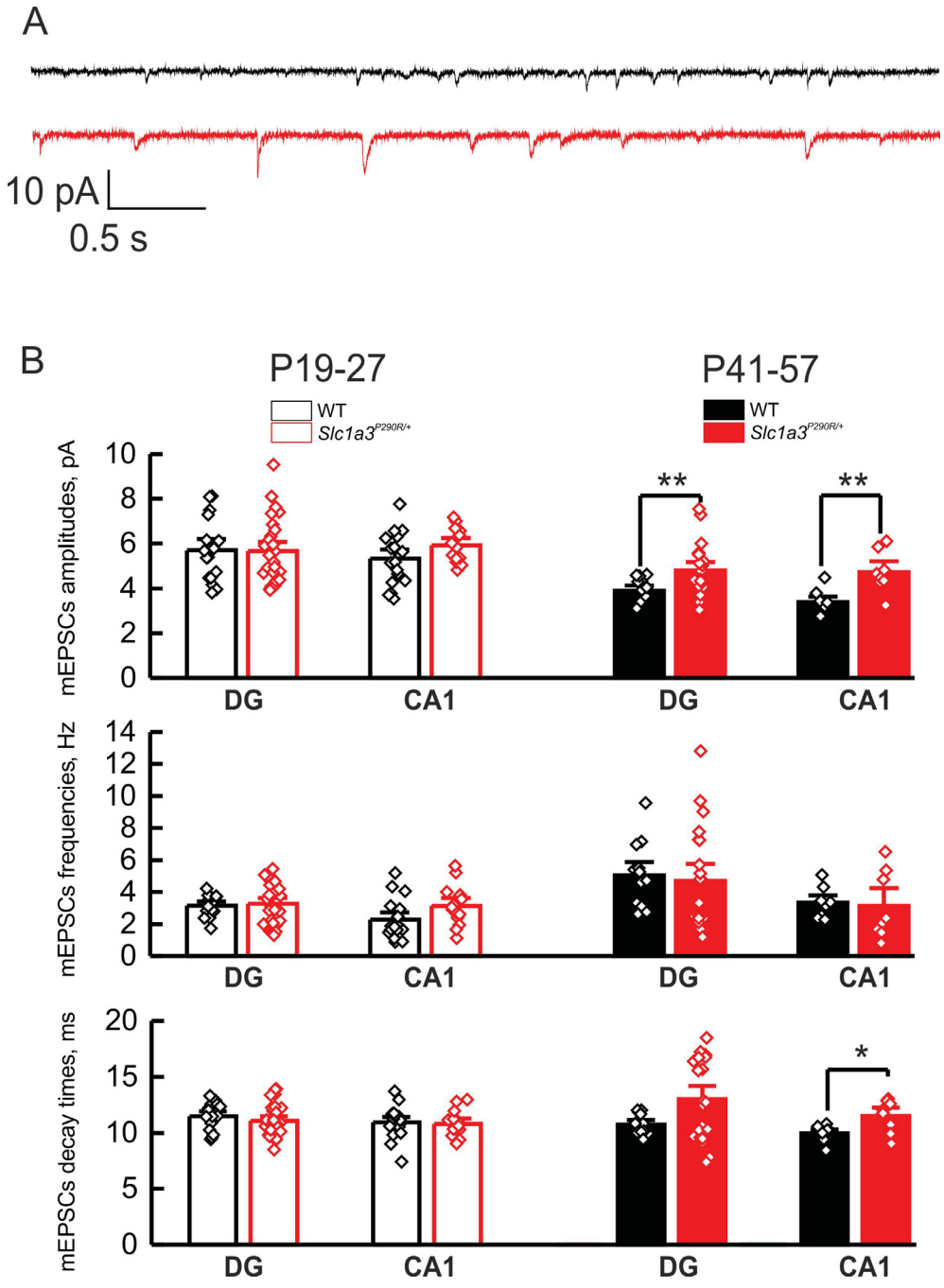


Figure 5.2: **AMPA receptor-mediated mEPSCs in the hippocampus of *Slc1a3*$^{P290R/+}$ mice before and after seizure onset.** A: representative whole-cell currents with mEPSCs from granule cell of WT (black) and *Slc1a3*$^{P290R/+}$ mice (red). B: amplitudes, frequencies and decay times are presented as bar graphs with mean ± SEM. Each data point represents the mean value obtained from one individual cell. In mutant mice, mEPSCs amplitudes are larger in both granule cells and CA1 pyramidal cells in the age of P41-57, after seizure onset, but not in the younger age of P19-27.

## 5.3 Decreased GABAergic inhibition in *Slc1a3*$^{P290R/+}$ granule cells

GABAergic inhibition is considered to be the main mechanism counterbalancing glutamatergic excitation, and, therefore, I tested a possible contribution of impaired GABAergic inhibition in the epileptic phenotype of *Slc1a3*$^{P290R/+}$ mice. Phasic and tonic GABA receptor-mediated currents were recorded from granule cells. Action potentials, AMPA and NMDA receptors were blocked by tetrodotoxin, CNQX, and AP-5 respectively. mIPSCs represent phasic synaptic inhibition provided by transient activation of synaptic $GABA_A$ receptors. There are no significant differences in mIPSCs amplitudes, frequencies or decay times between WT and mutants (Fig. 5.3).

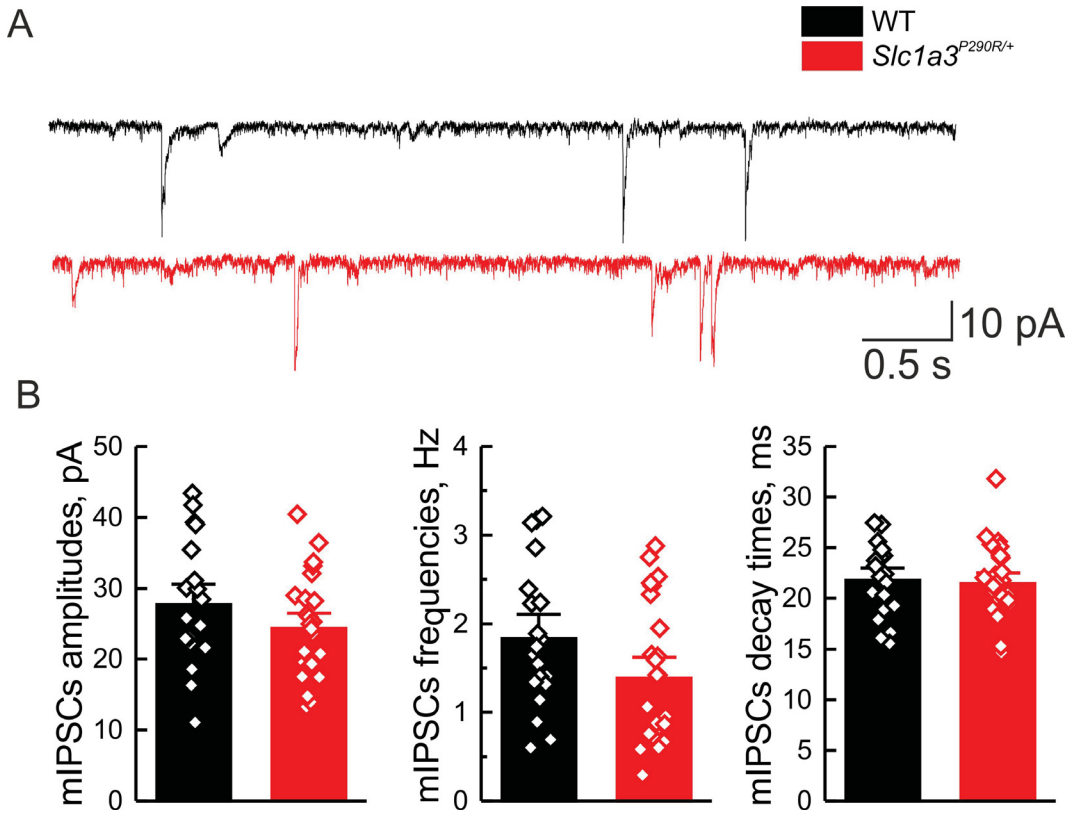


Figure 5.3: **Phasic GABAergic inhibition is not changed in hippocampal granule cells of *Slc1a3*$^{P290R/+}$ mice.** A: representative whole-cell currents with mIPSCs from WT (black) and *Slc1a3*$^{P290R/+}$ granule cells (red). B: amplitudes, frequencies and decay times are presented as bar graphs with mean ± SEM. Each data point represents the mean value obtained from one individual cell.

PTX was applied to the bath solution to measure the amplitudes of tonic GABAergic current generated by continuous activation of extrasynaptic $GABA_A$ receptors (Fig. 5.4). *Slc1a3*$^{P290R/+}$ granule cells show significantly decreased tonic current (mean: WT = 29.42 ± 6.24 pA, *Slc1a3*$^{P290R/+}$ = 13.71 ± 2.23 pA).

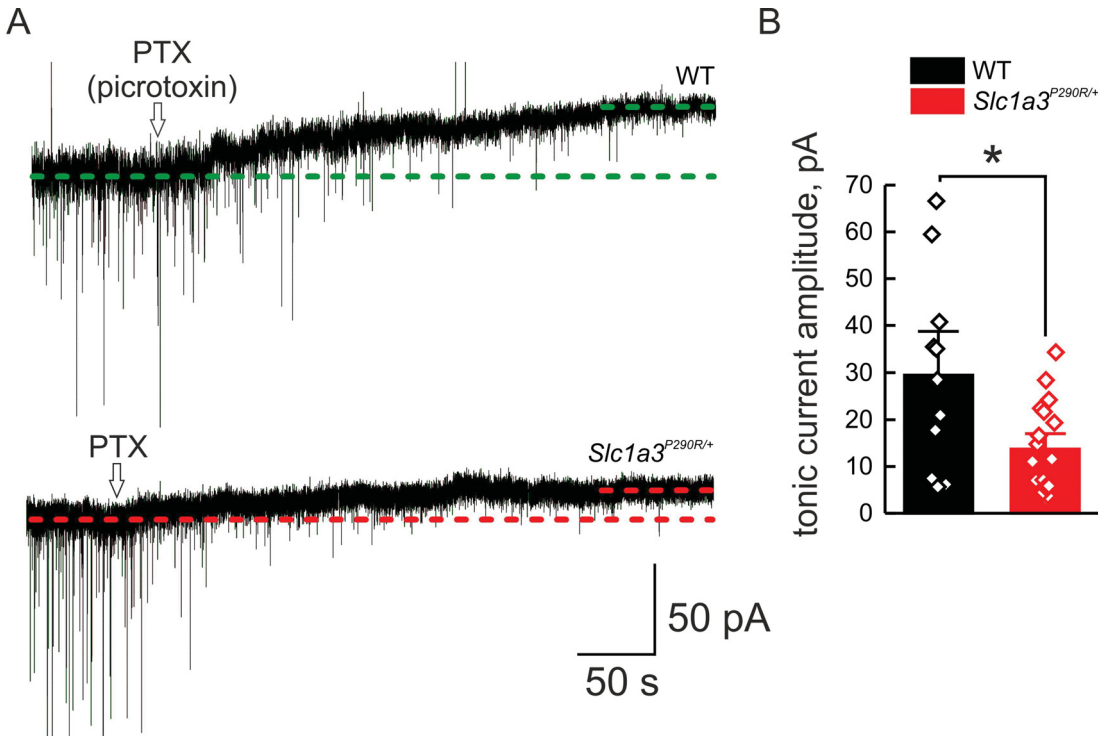


Figure 5.4: **Reduced tonic GABAergic inhibition in hippocampal granule cells of *Slc1a3*$^{P290R/+}$ mice.** A: representative whole-cell currents from WT and *Slc1a3*$^{P290R/+}$ granule cells. B: amplitudes of tonic conductances were calculated from holding current differences in the abscence and in the presence of the $GABA_A$-receptor blocker picrotoxin (PTX). The data is shown as bar graphs with mean ± SEM. Each data point represents the value obtained from one individual cell.

## 5.4 EAAT1/GLAST is predominantly expressed by NPCs in mouse hippocampi

Since NPCs are located in close proximity to granule cells, altered NPCs function may impair GABAergic inhibition in *Slc1a3*$^{P290R+}$ DG. Figure 5.5 shows representative confocal images from the DG of WT, *Slc1a3*$^{P290R/+}$, and *Slc1a3*$^{-/-}$ mice. An antibody against brain lipid-binding protein (BLBP) was used, due to its immunoreactivity being largely confined to the soma and nuclei of NPCs within the subgranular zone of DG. Control samples from *Slc1a3*$^{-/-}$ mice show no EAAT1/GLAST immunoreactivity.

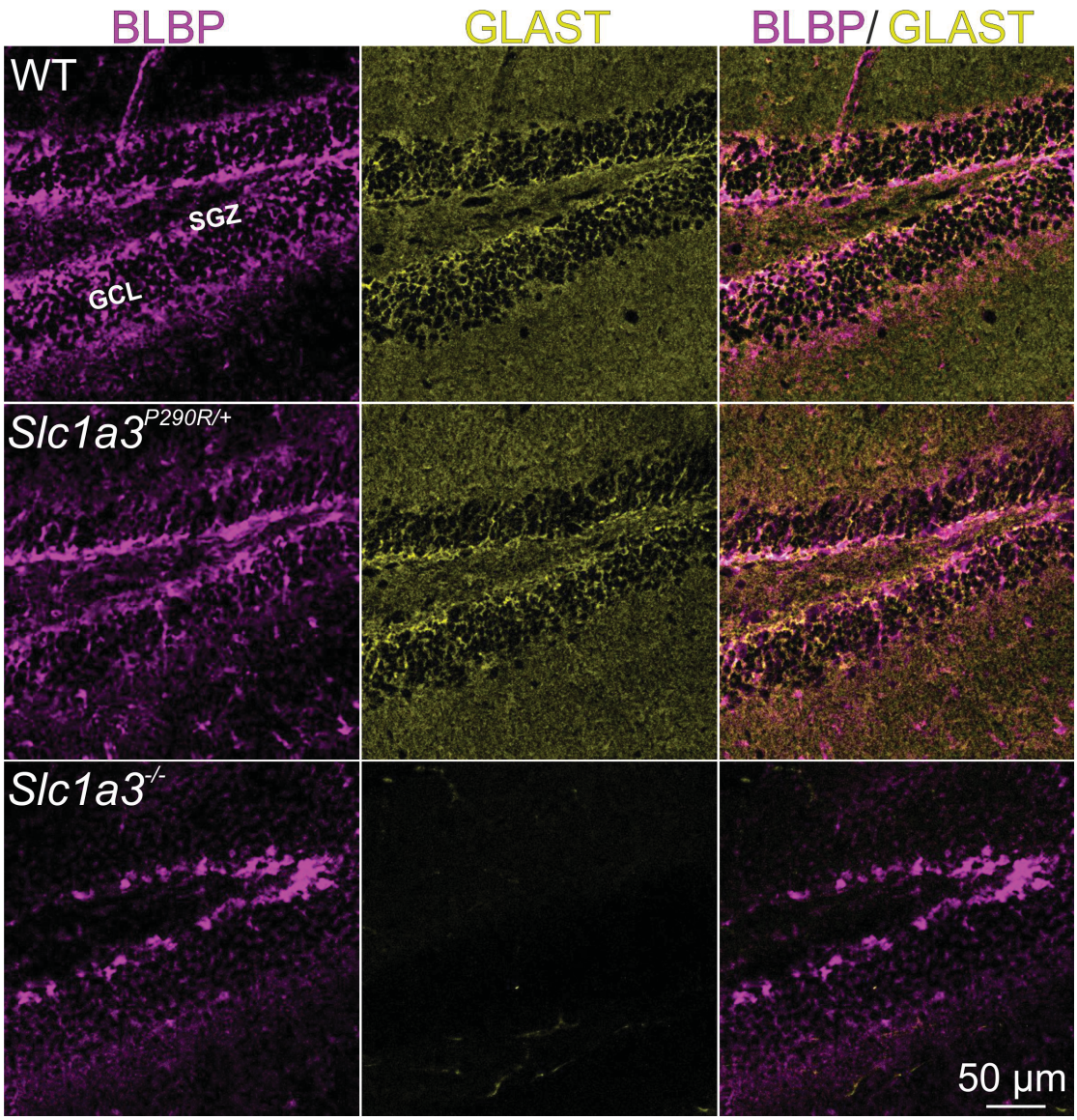


Figure 5.5: **Localization of EAAT1/GLAST in WT and *Slc1a3*$^{P290R/+}$ hippocampi.** Representative confocal images of WT, *Slc1a3*$^{P290R/+}$, and *Slc1a3*$^{-/-}$ slices showing the central region of the DG immunostained for BLBP (magenta), and EAAT1/GLAST (yellow). GCL: granule cell layer; SGZ: subgranular zone.

NPCs exhibit a specific EAAT1/GLAST expression signal in the membrane as well as in the vertical process, penetrating the granule cell layer (fig. 5.6). Staining of hippocampal astrocytes with an antibody against glial fibrillary (GFAP) shows no prominent co-localization of GFAP and EAAT1/GLAST.

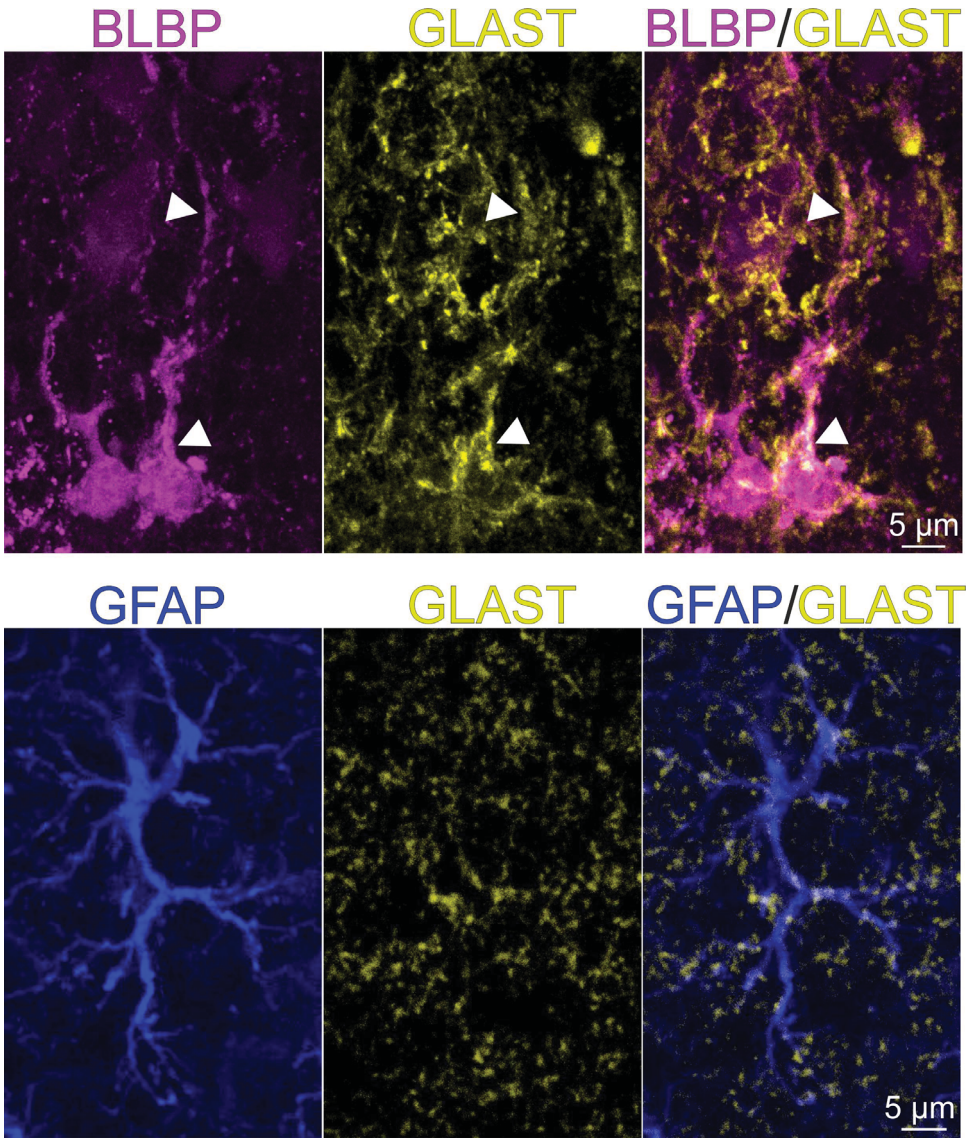


Figure 5.6: **EAAT1/GLAST expression in hippocampal astrocytes and NPCs.** Representative confocal images of NPCs, marked with BLBP (top) and astrocyte, marked with GFAP (bottom) showing EAAT1/GLAST expression. The main process of NPCs, expressing EAAT1/GLAST is indicated with arrowheads.

## 5.5 NPCs of mouse hippocampi express GAT-3

EAAT1/GLAST anion channels are one of the major determinants of $[Cl^-]_{int}$ in Bergmann glial cells (Untiet et al., 2017). Thus we tested $[Cl^-]_{int}$ in the hippocampal glial cells using fluorescence lifetime imaging with $Cl^-$ sensitive dye MQAE. We observed lower $[Cl^-]_{int}$ in NPCs of *Slc1a3*$^{P290R/+}$ mice (see chapter 3.6).

Changed $[Cl^-]_{int}$ could affect the driving force for secondary-active transporters utilizing transmembrane $Cl^-$ gradients, such as GABA transporters (Zhou and Danbolt, 2013). Sagittal hippocampal slices were immunostained for GABA transporter 3 (GAT-3) and BLBP to reveal the localization of GABA transporters in the NPCs (Fig. 5.7). The vertical process of NPCs penetrating granule cell layer of the DG exhibits colocalization of BLBP and GAT-3.

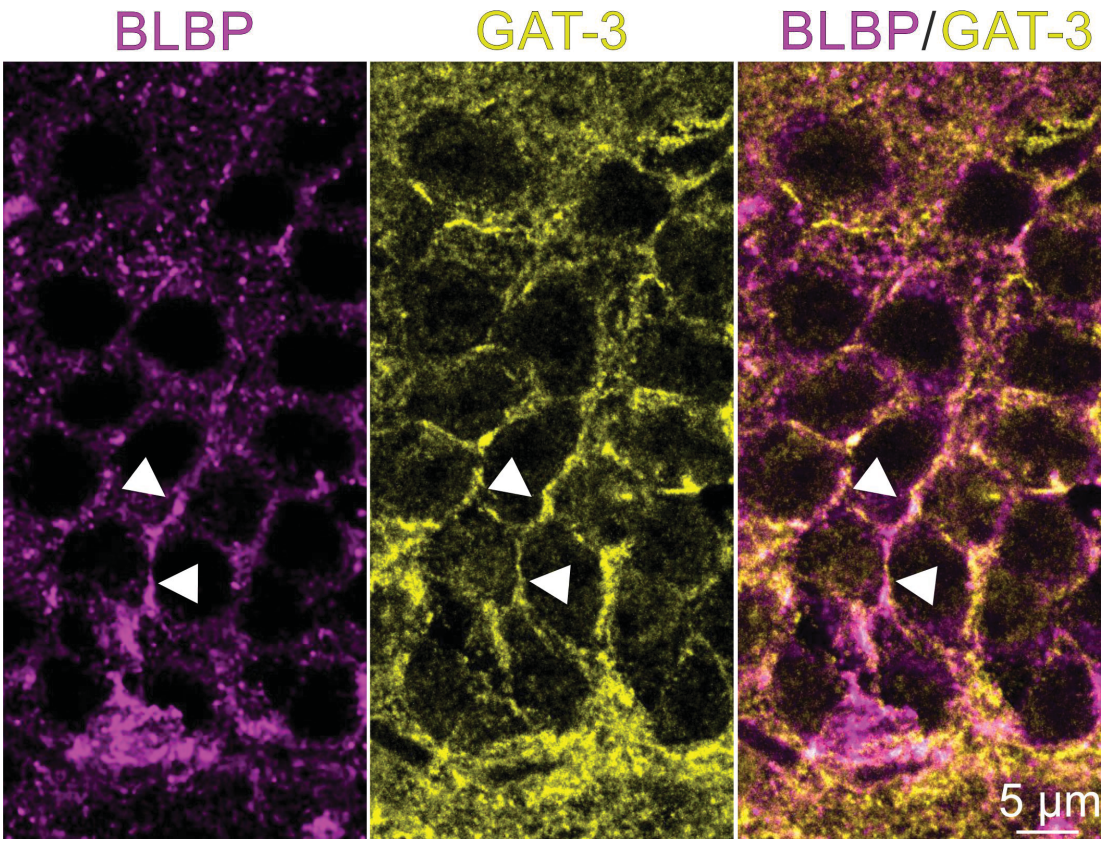


Figure 5.7: **GAT-3 expression in hippocampal NPCs.** Representative confocal images of NPC, marked with BLBP showing GAT-3 expression. The main process of NPC with radial morphology expresses GAT-3 and is indicated with arrowheads.

To test the relative protein expression of GAT-3 western blot analysis was performed. Upregulation of GAT-3 was observed in hippocampal lysates from *Slc1a3*$^{P290R/+}$ mice in the age of seizure onset (P20-28, Fig. 5.8). Decreased $[Cl^-]_{int}$ in NPCs of *Slc1a3*$^{P290R/+}$ mice may stimulate the GABA uptake via GAT-3 and change the extracellular GABA concentration, thereby affecting tonic GABAergic inhibition of granule cells. Decreased expression of GAT-3, observed in later ages (P38-42) may be explained by possible post-paroxysmal loss of glial cells in *Slc1a3*$^{P290R/+}$ mice, which requires further investigation.

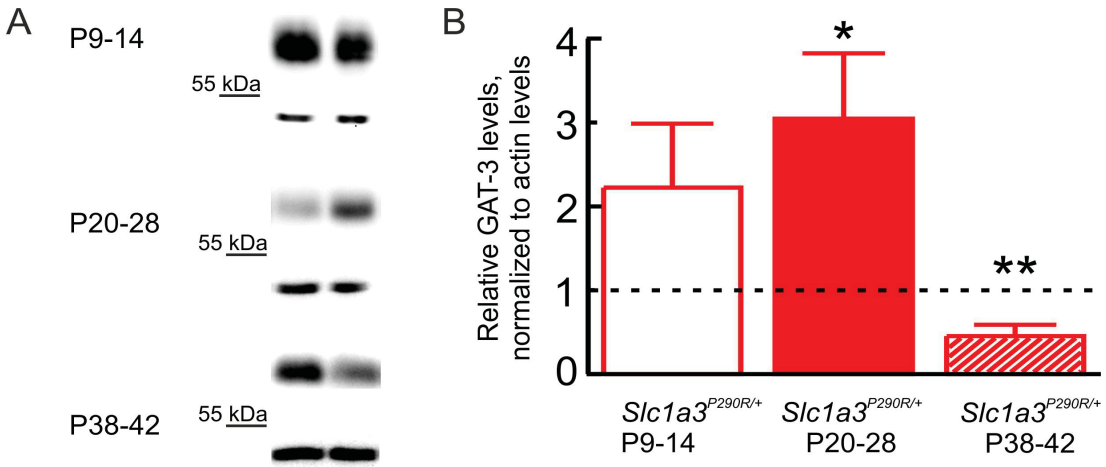


Figure 5.8: **Quantification of GAT-3 expression in the hippocampi of WT and *Slc1a3*$^{P290R/+}$ mice.** A: representative images of a western blot hippocampal lysate of WT and *Slc1a3*$^{P290R/+}$ from ages of P9-14, P20-28, and P38-42 incubated with GAT-3 and actin antibodies. B: Relative GAT-3 levels, normalized to actin levels, are plotted as bar graphs with mean ± SEM. The dashed line indicates the WT.

## 5.6 EAAT1/GLAST and EAAT2/GLT-1 protein expression levels in *Slc1a3*$^{P290R/+}$ hippocampi

P290R decreases human EAAT1 transporter density in the surface membrane (Winter et al., 2012) and *Slc1a3*$^{P290R/+}$ mice exhibit decreased EAAT1/GLAST expression in the cerebellum (Kovermann et al., 2020). To check if EAAT1/GLAST expression is decreased in *Slc1a3*$^{P290R/+}$ hippocampi, western

blot analysis of hippocampal lysates from WT and *Slc1a3*$^{P290R/+}$ mice was performed and evaluated in comparison to actin expression. Representative western blots for EAAT1/GLAST for ages before seizure onset (P9-14) and at seizure onset (P20-28), are shown in fig. 5.9; the bar graphs show the pooled values for all trials and animals used. Already during the second postnatal week, EAAT1/GLAST levels were reduced by about 19 % with a further reduction to 52 % observed at the age of seizure onset, probably due to NPCs loss, which needs to be investigated.

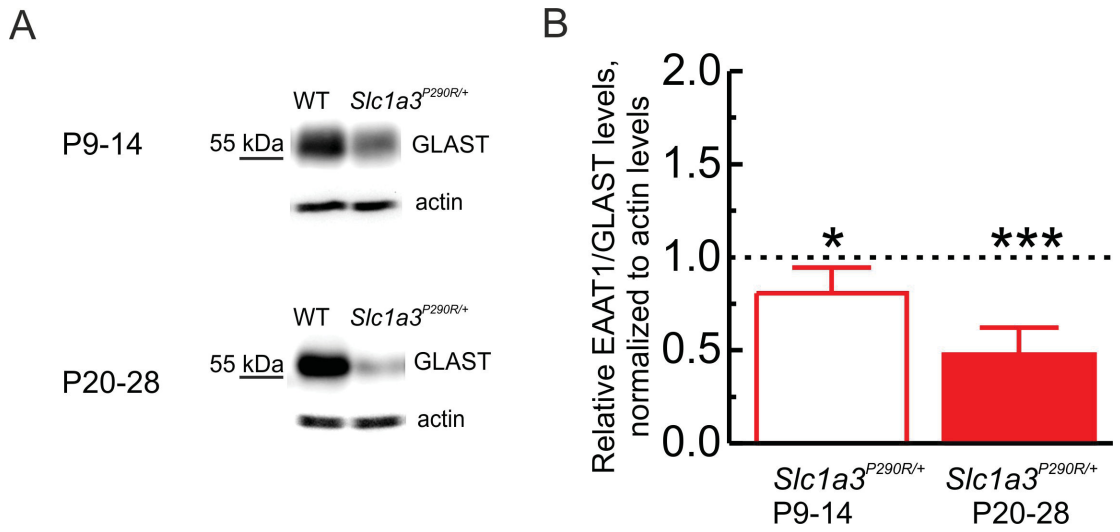


Figure 5.9: **Quantification of EAAT1/GLAST expression in the hippocampi of WT and *Slc1a3*$^{P290R/+}$ mice.** A: representative images of a western blot hippocampal lysate of WT and *Slc1a3*$^{P290R/+}$ from ages of P9-14, and P20-28 incubated with GLAST and actin antibodies. B: Relative EAAT1/GLAST levels, normalized to actin levels are plotted as bar graphs with mean ± SEM. The dashed line indicates the WT.

Despite the significant decrease of EAAT1/GLAST expression, by the end of the second postnatal week, no epileptic seizures were observed. To reveal a possible up-regulation of EAAT2/GLT-1, which could compensate for the loss of EAAT1/GLAST in *Slc1a3*$^{P290R/+}$ mice, the expression of EAAT2/GLT-1 was determined in WT and mutant hippocampal lysates. During the second postnatal week, a 3-fold increase in the expression levels of EAAT2/GLT-1 was observed, while there was no significant difference at P20-28 (Fig. 5.10). Thus

EAAT2/GLT-1 appears to compensate for the lack of GLAST and possible loss of NPCs in *Slc1a3*$^{P290R/+}$ hippocampi only during the second postnatal week.

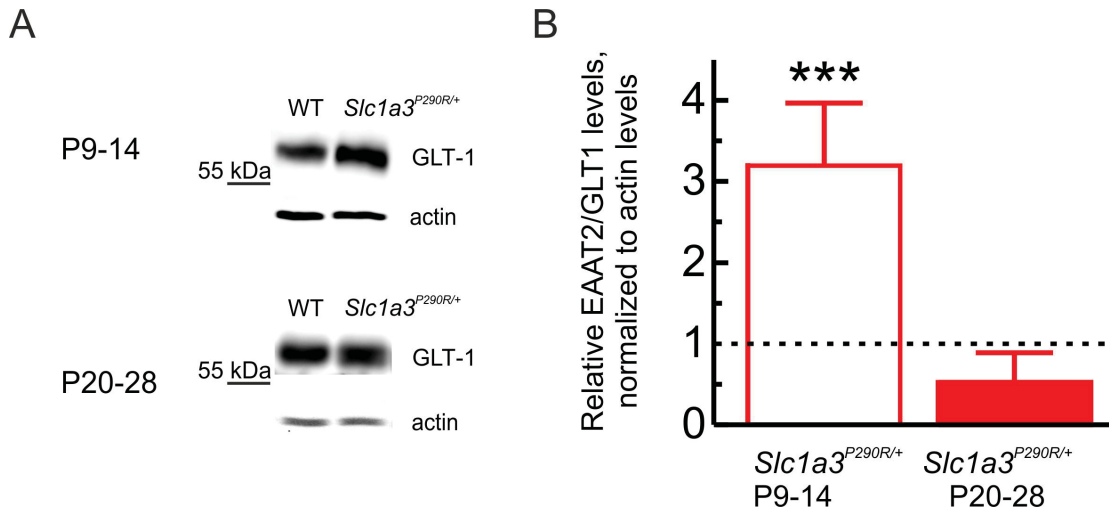


Figure 5.10: Q**uantification of EAAT2/GLT-1 expression in the hippocampi of WT and *Slc1a3*$^{P290R/+}$ mice.** A: representative images of a western blot hippocampal lysate of WT and *Slc1a3*$^{P290R/+}$ from ages of P9-14 and P20-28 incubated with αGLT-1 and αactin antibodies. B: Relative EAAT2/GLT-1 levels, normalized to actin levels are plotted as bar graphs with mean ± SEM. The dashed line indicates the WT.

## 5.7 Compensatory changes in *Slc1a3*$^{P290R/+}$ hippocampi

After surviving the specific paroxysmal period (P>68) *Slc1a3*$^{P290R/+}$ mice did not exhibit epileptic seizures anymore (Fig. 5.1). To reveal possible morphological changes of the hippocampal neurons, which would lead to an inability to further epileptic activity, dendritic spines of granule cells and CA1 pyramidal cells were visualized using Golgi-Cox staining. Analysis of spines in the secondary and tertiary dendrites in WT and *Slc1a3*$^{P290R/+}$ mice at P>68 showed a dramatic increase in the number of stubby and thin protrusions in mutant granule cells, concomitant with a significant decrease in the number of long thin spines compared to WT controls (Fig. 5.11). No significant difference in spine types composition was detected in *Slc1a3*$^{P290R/+}$ CA1 pyramidal cells, except a slight decrease in long thin protrusions. This finding suggests that *Slc1a3*$^{P290R/+}$ granule cells are affected at earlier stages and/or stronger than CA1 pyramidal cells.

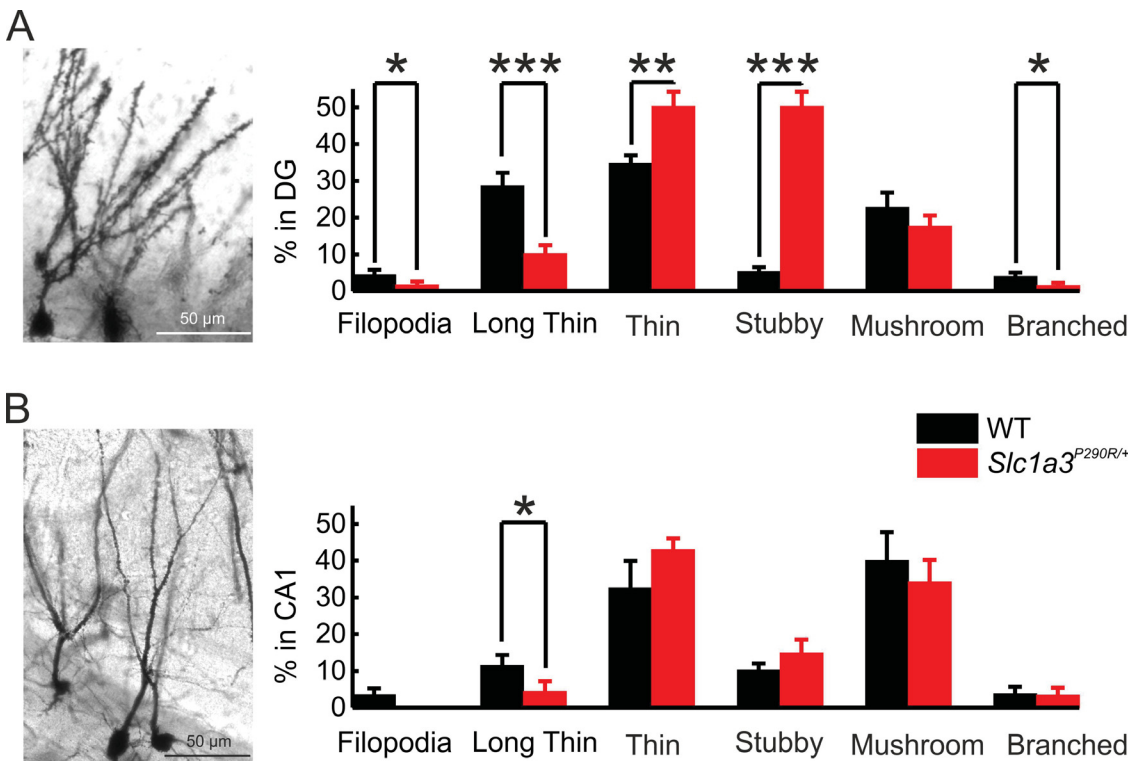


Figure 5.11: **The composition of spine types is altered within *Slc1a3*$^{P290R/+}$ hippocampi.** A: Representative Golgi–Cox stained DG granule cells. Secondary and tertiary dendrites of *Slc1a3*$^{P290R/+}$ granule cells demonstrate fewer Filopodia, Long Thin and Branched spine types, whereas the proportion of Thin and Stubby spines increases. B: Representative Golgi–Cox stained CA1 pyramidal cell. Composition of dendritic spine types is not changed except for a slight decrease of Long Thin spines. Data is shown as bar graphs with mean ± SEM.

Although there is no significant difference in the total protrusion density between genotypes, a general shrinkage of the dendritic spines in *Slc1a3*$^{P290R/+}$ granule cells and CA1 pyramidal cells was observed (Fig. 5.12).

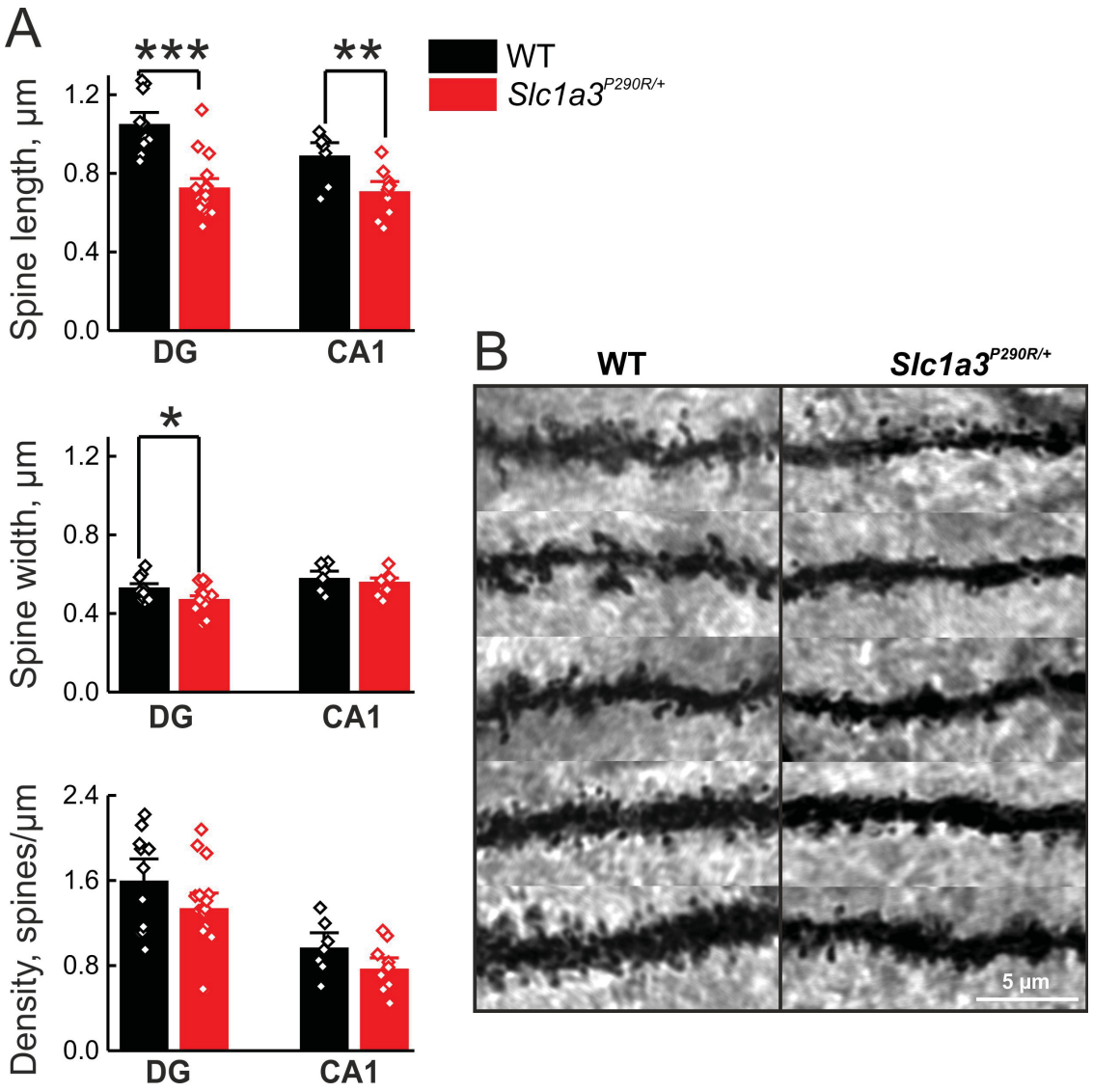


Figure 5.12: **Spine size and density within *Slc1a3*$^{P290R/+}$ hippocampi.** A: length and width of the dendritic spines is smaller in mutant hippocampi, although spine density is not altered. Data is shown as bar graphs with mean ± SEM. Each data point represents the mean value obtained from one individual 10 µm dendritic segment. B: representative Golgi–Cox stained secondary and tertiary dendrites of WT and *Slc1a3*$^{P290R/+}$ granule cells.

Epileptic activity may enforce presynaptic processes of granule cells to develop compensatory changes that result in glutamatergic presynaptic deficits. The amount of neurotransmitter released from the presynaptic terminal is dependent on levels of vesicular transporters (Daniels et al., 2004; Wilson et al., 2005; Wojcik et al., 2004). Fluorescence immunohistochemistry was used to detect the presynaptic marker VGLUT1 within mossy fiber terminals (Fig. 5.13). Quantitative analysis of VGLUT1 positive punctae in WT and *Slc1a3*$^{P290R/+}$ CA3 hippocampal subfields shows reduced VGLUT1 densities in the mutant mossy

fiber terminals, suggesting a possibly impaired excitatory neurotransmission in the CA3 region of the hippocampus following chronic epilepsy in *Slc1a3*$^{P290R/+}$ mice.

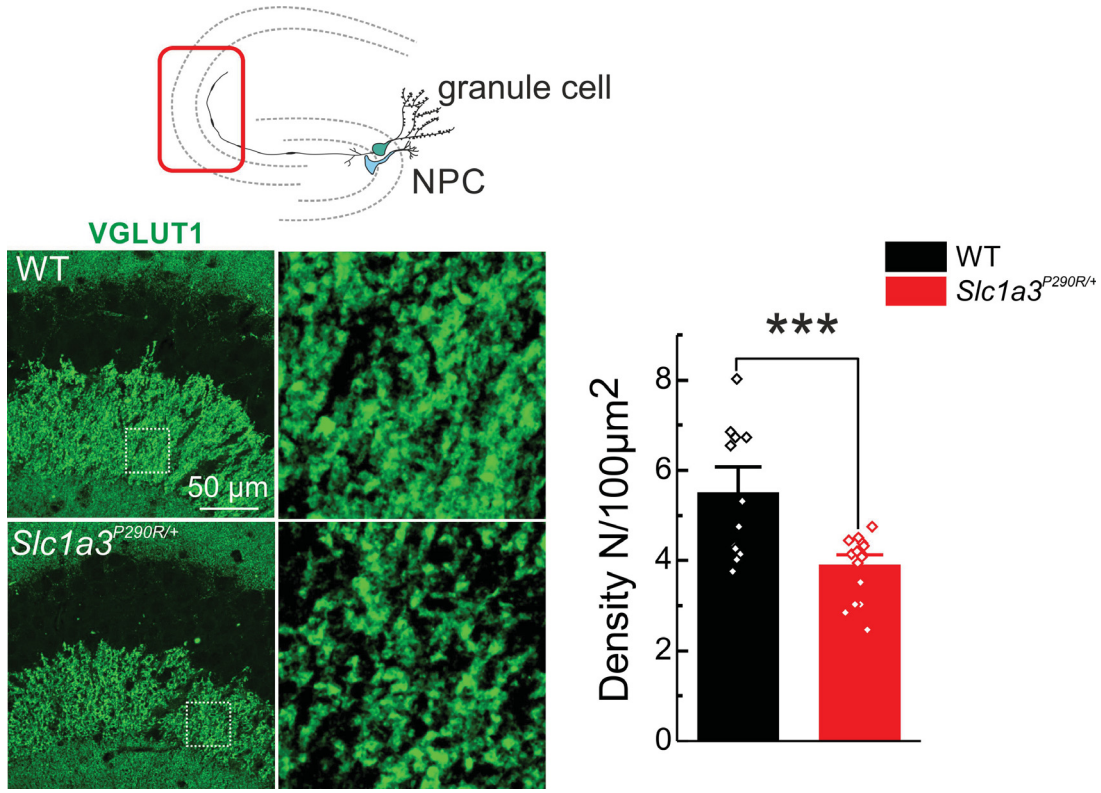


Figure 5.13: **Expression of VGLUT1 in granule cell mossy fiber terminals of WT and *Slc1a3*$^{P290R/+}$ hippocampi.** Representative confocal images of the CA3 region of WT and *Slc1a3*$^{P290R/+}$ mice showing decreased levels of VGLUT1 at P42-61. The density of manually calculated VGLUT1 punctae was significantly reduced in the CA3 region of mutant hippocampi. Data is shown as bar graphs with mean ± SEM. Each data point represents the mean value obtained from one individual brain slice.

Excitatory boutons in the hippocampus may contain either the VGLUT1 or VGLUT2 isoform of the vesicular glutamate transporter, and expression of the different isoforms may reflect glutamatergic presynaptic boutons that arise from different origins and/or have different release properties (Fremeau et al., 2004; Halasy et al., 2004). Thus, the density of VGLUT2 punctae was also assessed (Fig. 5 14).

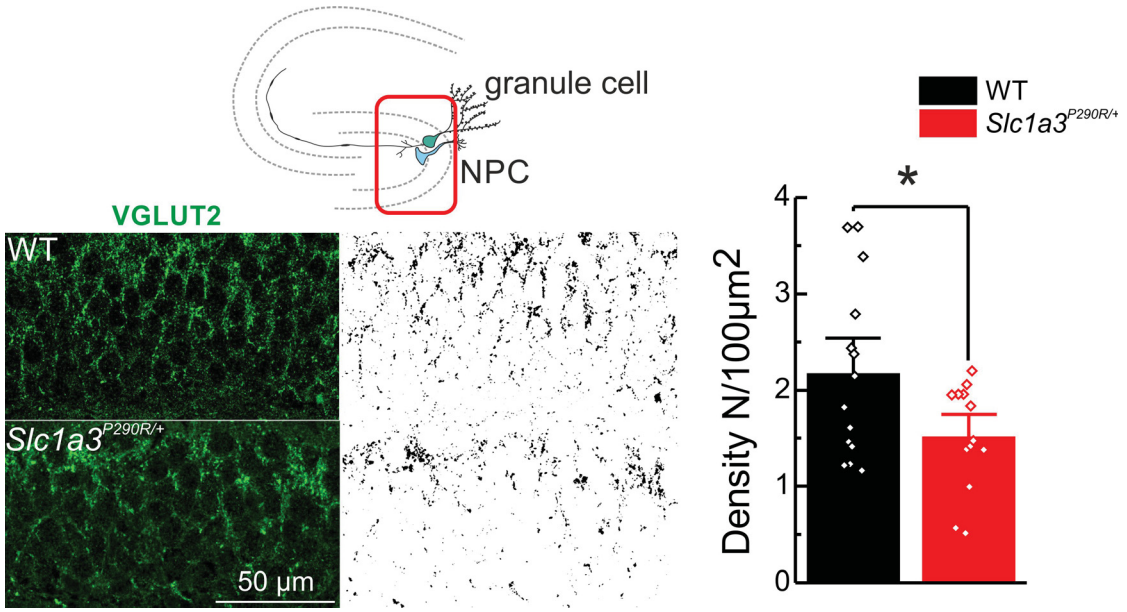


Figure 5.14: **Expression of VGLUT2 in the granule cell layer of WT and *Slc1a3*$^{P290R/+}$ hippocampi.** Representative confocal images of granule cell layer from WT and *Slc1a3*$^{P290R/+}$ mice, immunostained to VGLUT2. The density of VGLUT2 boutons is significantly reduced in the granule cell layer of mutant hippocampi. Data is shown as bar graphs with mean ± SEM. Each data point represents the mean value obtained from one individual brain slice.

Immunoreactivity for VGLUT2 is present in both the granule cell and molecular layers of the DG (Fremeau et al., 2001; Halasy et al., 2004; Kaneko and Fujiyama, 2002) and relatively low in the CA1 and CA3 regions (Fremeau et al., 2001). *Slc1a3*$^{P290R/+}$ DG immunostained for VGLUT2 shows reduced VGLUT2 punctae densities in the granule cell layer, possibly due to degeneration of the mossy cells of the ventral DG observed in both epileptic animals (Kienzler et al., 2009; Soussi et al., 2015) and humans (Blümcke et al., 2000).

## 5.8. Data

Table 5.1: **Values obtained from electrophysiological recordings from animals of different ages**

| | Age | Cells number of | Animals number of | Mean | Error (S.E.M.) | Normally distributed | Significance | Test |
|---|---|---|---|---|---|---|---|---|
| WT tonic current, pA | P20-30 | 11 | 5 | 29.42 | 6.24 | passed | p = 0.035 * | Two tailed Student's *t*-test (Welch correction) |
| *Slc1a3*$^{P290R/+}$ tonic current, pA | | 18 | 7 | 13.71 | 2.23 | passed | | |
| WT mIPSCs amplitude, pA | | 20 | 7 | 27.68 | 1.94 | passed | p = 0.168 | Two tailed Student's *t*-test |
| *Slc1a3*$^{P290R/+}$ mIPSCs amplitude, pA | | 25 | 8 | 24.38 | 1.43 | passed | | |
| WT mIPSCs frequency, Hz | | 20 | 7 | 1.83 | 0.18 | passed | p = 0.076 | Mann-Whitney Rank Sum Test |
| *Slc1a3*$^{P290R/+}$ mIPSCs frequency, Hz | | 25 | 8 | 1.38 | 0.16 | failed | | |
| WT mIPSCs decay time 90 to 10%, ms | | 20 | 7 | 21.79 | 0.79 | passed | p = 0.439 | Two tailed Student's *t*-test |
| *Slc1a3*$^{P290R/+}$ mIPSCs decay time 90 to 10%, ms | | 25 | 8 | 21.03 | 0.60 | passed | | |

| | | | | | | | | |
|---|---|---|---|---|---|---|---|---|
| WT mEPSCs amplitude granule cells, pA | P19-27 | 17 | 9 | 5.69 | 0.34 | passed | p = 0.952 | Two tailed Student's *t*-test |
| *Slc1a3*$^{P290R/+}$ mEPSCs amplitude granule cells, pA | | 28 | 6 | 5.67 | 0.27 | passed | | |
| WT mEPSCs frequency granule cells, Hz | | 16 | 9 | 3.16 | 0.17 | passed | p = 0.775 | Two tailed Student's *t*-test |
| *Slc1a3*$^{P290R/+}$ mEPSCs frequency granule cells, Hz | | 29 | 6 | 3.26 | 0.24 | passed | | |
| WT mEPSCs decay time 90 to 10% granule cells, ms | | 17 | 9 | 11.48 | 0.28 | passed | p = 0.320 | Two tailed Student's *t*-test |
| *Slc1a3*$^{P290R/+}$ mEPSCs decay time 90 to 10% granule cells, ms | | 29 | 6 | 11.08 | 0.26 | passed | | |
| WT mEPSCs amplitude CA1 pyramidal neurons, pA | | 18 | 6 | 5.33 | 0.27 | passed | p = 0.125 | Two tailed Student's *t*-test |
| *Slc1a3*$^{P290R/+}$ mEPSCs amplitude CA1 pyramidal neurons, pA | | 13 | 5 | 5.91 | 0.22 | passed | | |
| WT mEPSCs frequency CA1 pyramidal neurons, Hz | | 17 | 6 | 2.28 | 0.30 | failed | p = 0.050 | Mann-Whitney Rank Sum Test |
| *Slc1a3*$^{P290R/+}$ mEPSCs frequency CA1 pyramidal neurons, Hz | | 14 | 5 | 3.13 | 0.34 | passed | | |
| WT mEPSCs decay time 90 to 10% CA1 pyramidal neurons, ms | | 18 | 6 | 10.92 | 0.33 | passed | p = 0.806 | Two tailed Student's *t*-test |
| *Slc1a3*$^{P290R/+}$ mEPSCs decay time 90 to 10% CA1 pyramidal neurons, ms | | 14 | 5 | 10.81 | 0.31 | passed | | |

| | | | | | | | | |
|---|---|---|---|---|---|---|---|---|
| WT mEPSCs amplitude granule cells, pA | P41-57 | 13 | 5 | 3.90 | 0.15 | passed | p = 0.005 ** | Two tailed Student's *t*-test (Welch correction) |
| *Slc1a3*$^{P290R/+}$ mEPSCs amplitude granule cells, pA | | 21 | 4 | 4.80 | 0.26 | passed | | |
| WT mEPSCs frequency granule cells, Hz | | 13 | 5 | 5.05 | 0.55 | passed | p = 0.339 | Mann-Whitney Rank Sum Test |
| *Slc1a3*$^{P290R/+}$ mEPSCs frequency granule cells, Hz | | 21 | 4 | 4.70 | 0.70 | failed | | |
| WT mEPSCs decay time 90 to 10% granule cells, ms | | 12 | 5 | 10.71 | 0.28 | passed | p = 0.141 | Mann-Whitney Rank Sum Test |
| *Slc1a3*$^{P290R/+}$ mEPSCs decay time 90 to 10% granule cells, ms | | 21 | 4 | 13.00 | 0.79 | failed | | |
| WT mEPSCs amplitude CA1 pyramidal neurons, pA | | 9 | 3 | 3.35 | 0.16 | passed | p = 0.003 ** | Two tailed Student's *t*-test (Welch correction) |
| *Slc1a3*$^{P290R/+}$ mEPSCs amplitude CA1 pyramidal neurons, pA | | 8 | 3 | 4.72 | 0.32 | passed | | |
| WT mEPSCs frequency CA1 pyramidal neurons, Hz | | 9 | 3 | 3.33 | 0.31 | passed | p = 0.809 | Two tailed Student's *t*-test (Welch correction) |
| *Slc1a3*$^{P290R/+}$ mEPSCs frequency CA1 pyramidal neurons, Hz | | 8 | 3 | 3.13 | 0.75 | passed | | |
| WT mEPSCs decay time 90 to 10% CA1 pyramidal neurons, ms | | 9 | 3 | 9.94 | 0.23 | passed | p = 0.021 * | Two tailed Student's *t*-test (Welch correction) |
| *Slc1a3*$^{P290R/+}$ mEPSCs decay time 90 to 10%, CA1 pyramidal cells, ms | | 8 | 3 | 10.94 | 0.97 | passed | | |

Table 5.2: **Values obtained from Golgi-Cox stained brain slices and characterization of spine types and morphology**

| | Segments number of | Cells number of | Slices number of | Animals number of | Mean | Error (S.E.M.) | Normally distributed | Significance | Test |
|---|---|---|---|---|---|---|---|---|---|
| WT granule cells' spine length, µm | 11 | 11 | 5 | 2 | 1.05 | 0.05 | passed | p < 0.001 *** | Two tailed Student's *t*-test |
| *Slc1a3*$^{P290R/+}$ granule cells' spine length, µm | 16 | 13 | 5 | 3 | 0.70 | 0.03 | passed | | |
| WT granule cells' spine width, µm | 11 | 11 | 5 | 2 | 0.53 | 0.02 | passed | p = 0.029 * | Two tailed Student's *t*-test |
| *Slc1a3*$^{P290R/+}$ granule cells' spine width, µm | 17 | 13 | 5 | 3 | 0.47 | 0.02 | passed | | |
| WT granule cells' spine density, protrusions/um | 11 | 11 | 5 | 2 | 1.60 | 0.14 | passed | p = 0.126 | Two tailed Student's *t*-test |
| *Slc1a3*$^{P290R/+}$ granule cells' spine density, protrusions/um | 17 | 13 | 5 | 3 | 1.38 | 0.10 | passed | | |
| WT granule cells' filopodia spine % | 11 | 11 | 5 | 2 | 4.42 | 1.35 | passed | p = 0.017 * | Mann-Whitney Rank Sum Test |
| *Slc1a3*$^{P290R/+}$ granule cells' filopodia spine % | 16 | 13 | 5 | 3 | 0.94 | 0.51 | failed | | |

| | | | | | | | | | |
|---|---|---|---|---|---|---|---|---|---|
| WT granule cells' long thin spine % | 11 | 11 | 5 | 2 | 28.69 | 3.55 | passed | p < 0.001 *** | Two tailed Student's *t*-test (Welch correction) |
| *Slc1a3*$^{P290R/+}$ granule cells' long thin spine % | 16 | 13 | 5 | 3 | 8.39 | 1.69 | passed | | |
| WT granule cells' thin spine % | 11 | 11 | 5 | 2 | 34.82 | 2.15 | passed | p = 0.002 ** | Two tailed Student's *t*-test (Welch correction) |
| *Slc1a3*$^{P290R/+}$ granule cells' thin spine % | 17 | 13 | 5 | 3 | 50.27 | 3.94 | passed | | |
| WT granule cells' stubby spine % | 11 | 11 | 5 | 2 | 5.30 | 1.26 | passed | p < 0.001 *** | Two tailed Student's *t*-test (Welch correction) |
| *Slc1a3*$^{P290R/+}$ granule cells' stubby spine % | 17 | 13 | 5 | 3 | 50.27 | 3.94 | passed | | |
| WT granule cells' mushroom spine % | 11 | 11 | 5 | 2 | 22.79 | 4.03 | passed | p = 0.298 | Two tailed Student's *t*-test |
| *Slc1a3*$^{P290R/+}$ granule cells' mushroom spine % | 17 | 13 | 5 | 3 | 17.58 | 2.96 | passed | | |
| WT granule cells' branched spine % | 11 | 11 | 5 | 2 | 4.02 | 0.99 | passed | p = 0.007 * | Mann-Whitney Rank Sum Test |
| *Slc1a3*$^{P290R/+}$ granule cells' branched spine % | 16 | 13 | 5 | 3 | 1.47 | 0.73 | failed | | |

| | | | | | | | | | |
|---|---|---|---|---|---|---|---|---|---|
| WT CA1 pyramidal cells spine length, µm | 7 | 5 | 3 | 2 | 0.88 | 0.05 | passed | p = 0.009 ** | Two tailed Student's *t*-test |
| *Slc1a3*$^{P290R/+}$ CA1 pyramidal cells spine length, µm | 10 | 7 | 3 | 3 | 0.70 | 0.04 | passed | | |
| WT CA1 pyramidal cells spine width, µm | 7 | 5 | 3 | 2 | 0.57 | 0.03 | passed | p = 0.530 | Two tailed Student's *t*-test |
| *Slc1a3*$^{P290R/+}$ CA1 pyramidal cells spine width, µm | 10 | 7 | 3 | 3 | 0.56 | 0.02 | passed | | |
| WT CA1 pyramidal cells spine density, protrusions/um | 7 | 5 | 3 | 2 | 0.97 | 0.10 | passed | p = 0.107 | Two tailed Student's *t*-test |
| *Slc1a3*$^{P290R/+}$ CA1 pyramidal cells spine density, protrusions/um | 10 | 7 | 3 | 3 | 0.77 | 0.07 | passed | | |
| WT CA1 pyramidal cells filopodia spine % | 7 | 5 | 3 | 2 | 3.49 | 0 | failed | p = 0.103 | Mann-Whitney Rank Sum Test |
| *Slc1a3*$^{P290R/+}$ CA1 pyramidal cells filopodia spine % | 10 | 7 | 3 | 3 | 0 | 0 | failed | | |
| WT CA1 pyramidal cells long thin spine % | 7 | 5 | 3 | 2 | 11.41 | 2.93 | passed | p = 0.049 * | Mann-Whitney Rank Sum Test |
| *Slc1a3*$^{P290R/+}$ CA1 pyramidal cells long thin spine % | 10 | 7 | 3 | 3 | 4.38 | 2.77 | failed | | |

| | | | | | | | | | |
|---|---|---|---|---|---|---|---|---|---|
| WT CA1 pyramidal cells thin spine % | 7 | 5 | 3 | 2 | 32.54 | 7.41 | passed | p = 0.229 | Two tailed Student's *t*-test (Welch correction) |
| *Slc1a3*$^{P290R/+}$ CA1 pyramidal cells thin spine % | 10 | 7 | 3 | 3 | 43.00 | 3.10 | passed | | |
| WT CA1 pyramidal cells stubby spine % | 7 | 5 | 3 | 2 | 8.77 | 2.12 | passed | p = 0.166 | Two tailed Student's *t*-test (Welch correction) |
| *Slc1a3*$^{P290R/+}$ CA1 pyramidal cells stubby spine % | 10 | 7 | 3 | 3 | 14.93 | 3.63 | passed | | |
| WT CA1 pyramidal cells mushroom spine % | 7 | 5 | 3 | 2 | 40.10 | 7.61 | passed | p = 0.549 | Two tailed Student's *t*-test |
| *Slc1a3*$^{P290R/+}$ CA1 pyramidal cells mushroom spine % | 10 | 7 | 3 | 3 | 34.22 | 6.01 | passed | | |
| WT CA1 pyramidal cells branched spine % | 7 | 5 | 3 | 2 | 3.68 | 1.96 | failed | p = 0.867 | Mann-Whitney Rank Sum Test |
| *Slc1a3*$^{P290R/+}$ CA1 pyramidal cells branched spine % | 10 | 7 | 3 | 3 | 3.47 | 1.91 | failed | | |

Table 5.3: **Values obtained from immunohistochemical analysis**

| | Age | Segments number of | Slices number of | Animals number of | Mean | Error (S.E.M.) | Normally distributed | Significance | Test |
|---|---|---|---|---|---|---|---|---|---|
| WT granule cell' mossy fibers VGLUT1 density, N/100 µm$^2$ | P42-61 | 12 | 4 | 2 | 5.45 | 0.42 | passed | p = 0.003 ** | Two tailed Student's *t*-test (Welch correction) |
| *Slc1a3*$^{P290R/+}$ granule cells' mossy fibers VGLUT1 density, N/100 µm$^2$ | | 15 | 5 | 2 | 3.85 | 0.18 | passed | | |
| WT granule cells' VGLUT2 density, N/100 µm$^2$ | | 14 | 7 | 2 | 2.17 | 0.25 | passed | p = 0.033 * | Two tailed Student's *t*-test (Welch correction) |
| *Slc1a3*$^{P290R/+}$ granule cells' mossy fibers VGLUT2 density, N/100 µm$^2$ | | 13 | 7 | 2 | 1.52 | 0.15 | passed | | |

Table 5.4: **Relative protein expression levels**

| Protein | Genotype | Age | Animals number of | Mean | SD | 95% CI | Significance (Two tailed Student's *t*-test) |
|---|---|---|---|---|---|---|---|
| EAAT1/GLAST vs. actin | WT | P9-14 | 7 | 1.00 | 0.51 | 1.27 | p = 0.044 * |
| | *Slc1a3*$^{P290R/+}$ | | 5 | 0.81 | 0.34 | 0.63 | |
| | WT | P20-28 | 3 | 2.36 | 0.92 | 3.04 | p < 0.001 *** |
| | *Slc1a3*$^{P290R/+}$ | | 3 | 1.12 | 0.61 | 0.67 | |
| EAAT2/GLT1 vs. actin | WT | P9-14 | 7 | 0.62 | 0.17 | 0.50 | p < 0.001 *** |
| | *Slc1a3*$^{P290R/+}$ | | 5 | 1.83 | 0.81 | 2.39 | |
| | WT | P20-28 | 3 | 2.00 | 1.31 | 3.15 | p = 0.088 |
| | *Slc1a3*$^{P290R/+}$ | | 3 | 1.04 | 1.10 | 0.08 | |

| | | | | | | | |
|---|---|---|---|---|---|---|---|
| GAT-3 vs. actin | WT | P9-14 | 3 | 1.41 | 0.43 | 0.49 | p = 0.127 |
| | *Slc1a3*$^{P290R/+}$ | | 3 | 3.50 | 1.89 | 2.13 | |
| | WT | P20-28 | 3 | 0.55 | 0.31 | 0.55 | p = 0.022 * |
| | *Slc1a3*$^{P290R/+}$ | | 3 | 1.67 | 1.13 | 1.67 | |
| | WT | P38-42 | 3 | 0.61 | 0.20 | 0.61 | p < 0.002 ** |
| | *Slc1a3*$^{P290R/+}$ | | 3 | 0.28 | 0.20 | 0.28 | |

# 6 Discussion

## 6.1. The imbalance between excitation and inhibition within the hippocampal network of *Slc1a3*$^{P290R/+}$ mice

EA6 is associated with missense mutations in the *SLC1A3* gene and characterized by paroxysmal cerebellar incoordination and epilepsy. An EA6 animal model, *Slc1a3*$^{P290R/+}$ mice, exhibits tonic-clonic seizures with onset during the fourth postnatal week (Fig 5.1). Epileptogenesis is the gradual progression of the brain from a normal to an epileptic state due to abnormal synchronous neuronal network activity in a focal area or throughout the entire brain. Hippocampal excitatory synaptic loops are involved in creating an underlying predisposition of the hippocampus and associated limbic structures to generate seizures (Heinemann et al., 1992; Lothman et al., 1992). The current study demonstrates an imbalance between GABAergic inhibition and glutamatergic excitation in the hippocampus of *Slc1a3*$^{P290R/+}$ mice. Whole-cell patch-clamp recordings from acute brain slices revealed decreased GABAergic tonic inhibition in the *Slc1a3*$^{P290R/+}$ DG, followed by elevated AMPA receptor-mediated excitation of the principal hippocampal neurons. Several findings support the hypothesis that this imbalance could govern epileptic seizures in the mutant animals.

Hippocampi of *Slc1a3*$^{P290R/+}$ mice exhibited elevated densities of ionotropic glutamate AMPA receptors (Fig. 3.2, unpublished data), suggesting excessive AMPA receptor-mediated glutamatergic excitation. Miniature postsynaptic currents, both excitatory (mEPSCs) and inhibitory (mIPSCs), are commonly believed to reflect the postsynaptic action of the neurotransmitter, contained in a single vesicle and released by spontaneous exocytosis (Edwards et al., 1990). The amplitude of the mPSCs thus reflects the number of postsynaptic receptors (Nusser et al., 1997) and the amount of neurotransmitter in the synaptic vesicle (Frerking et al., 1995). The frequency of mPSCs is determined by the total number of presynaptic axon terminals forming synapses on the neuron and the quantal-release probability at the individual synapses. Decay times of the mPSCs are primarily determined by the receptor subunit composition (Eyre et al., 2012) and can be affected by the spatio-temporal profile of the

neurotransmitter in the synaptic cleft (Auger et al., 1998; Williams et al., 1998). Whole-cell patch-clamp recordings from granule cells and CA1 pyramidal cells of *Slc1a3*$^{P290R/+}$ mice revealed increased amplitudes of AMPA receptor-mediated mEPSCs, in agreement with the observed higher AMPA receptors densities. AMPA receptors play an important role in epileptic synchronization and the spread of epileptiform activity across the hippocampal network. Inhibition of AMPA receptors has reduced or abolished epileptiform activity, conferring seizure protection in a broad range of animal seizure models (Rogawski, 2013). Moreover, the receptor's antagonist perampanel has been used clinically to treat patients with tonic-clonic seizures (French et al., 2012, 2015).

At the age of seizure onset (P19-27), *Slc1a3*$^{P290R/+}$ mice did not exhibit the increased AMPA receptor-mediated mEPSCs (Fig. 5.2), which were observed only after seizures onset (P41-57). Since the impaired AMPA receptor-mediated excitation does not appear before or simultaneously with the onset of the spontaneous seizures, it can not be the initiating stimulus for seizures in *Slc1a3*$^{P290R/+}$ mice, nevertheless, it could contribute to seizure maintenance.

In contrast, impairment of GABAergic inhibition was detected in the mutant hippocampus already at the age of seizure onset (Fig. 5.4), suggesting its role in seizure initiation. GABAergic inhibition has been traditionally viewed as the main mechanism counterbalancing glutamatergic excitation and preventing hypersynchronous neuronal discharges. Granule cells are known to exhibit strong GABAergic inhibition and at the same time play the role of a hippocampal gate, regulating incoming excitation. Although mIPSCs were not altered in *Slc1a3*$^{P290R/+}$ granule cells, picrotoxin application evoked significantly lower baseline current shifts, indicating a decreased GABAergic tonic inhibition.

In adult murine granule cells tonic inhibition appears to be more powerful than phasic, since tonic current, mediated by δ-subunit-containing extrasynaptic $GABA_A$ receptors has been ~4 times larger, than summed phasic current, produced by mIPSCs occurring at a frequency of ~10 Hz (Nusser and Mody, 2002; Wlodarczyk et al., 2013). Moreover, an impaired tonic inhibition alone seems sufficient to induce epilepsy, since several mouse models (Maguire et al., 2005; Peng et al., 2004; Spigelman et al., 2002; Zhang et al., 2007) and

human epilepsies are associated with mutations in genes encoding extrasynaptic $GABA_A$ receptors (Dibbens et al., 2004; Feng et al., 2006; Eugène et al., 2007; Mulley et al., 2005). Thus, altered tonic inhibition of granule cells may have a fundamental role in the initiation and propagation of seizures in the epileptic *Slc1a3*$^{P290R/+}$ mice.

## 6.2 The role of P290R EAAT1/GLAST in the pathophysiology of hippocampal NPCs

Impaired neuronal GABAergic tonic inhibition in *Slc1a3*$^{P290R/+}$ mice is expected to result from the incorrect function of glial cells since the P290R mutation affects the glial glutamate transporter EAAT1/GLAST (Jen et al., 2005; Winter et al., 2012; Kovermann et al., 2020). Immunostaining of hippocampal slices revealed EAAT1/GLAST expression in the NPCs of the DG. Although EAAT1/GLAST is known to be also expressed in hippocampal astrocytes, GFAP-stained astrocytic processes have not shown signal colocalization with GLAST, possibly due to the moderate EAAT1/GLAST expression levels in mature astrocytes (Furuta et al., 1997), while maximal EAAT1/GLAST expression has been observed in immature astrocytes (Shibata et al., 1997; Raponi et al., 2007).

In adult mammals, there is a variety of glial cell types with high EAAT1/GLAST expression, such as Müller's glia (Rauen et al., 1996) and cerebellar Bergmann's glia (Rothstein et al., 1994). Similarly to a subpopulation of hippocampal NPCs, both of these cell types exhibit radial glia morphology and a dominating role of EAAT1/GLAST in the overall glutamate clearing in the retina and cerebellum is well established (Tse et al., 2014; Miyazaki et al., 2017). In contrast, hippocampal NPCs are characterized mainly from the perspective of their progenitor capacity, while the role of EAAT1/GLAST in these cells still requires further investigation.

The speculated role of EAAT1/GLAST in hippocampal NPCs is the regulation of the extracellular glutamate levels, which control the migration of newborn granule cells (Shibata et al., 1997) and the activity of the neighboring granule cells. Considering the dual function of EAAT1/GLAST as transporter and channel, its alternative role in the regulation of the internal chloride

concentration ($[Cl^-]_{int}$) might be proposed. $[Cl^-]_{int}$ affects cellular volume, particularly important for the cells with the capacity to divide; and nonsynaptic GABA signaling, since high $[Cl^-]_{int}$ is essential for glial depolarization upon $GABA_A$ receptors activation. Glial $[Cl^-]_{int}$ can also indirectly control the activity of granule cells by affecting ambient GABA ($[GABA]_{ext}$). GABA transporters (GATs) couple GABA uptake to $Na^+$ and $Cl^-$ gradients (Zhou and Danbolt, 2013), so that their total driving force is composed of the driving forces for each transported molecule (Richerson and Wu, 2003). Thus, reduced $[Cl^-]_{int}$ can accelerate the driving force of the GATs, influencing thereby $[GABA]_{ext}$.

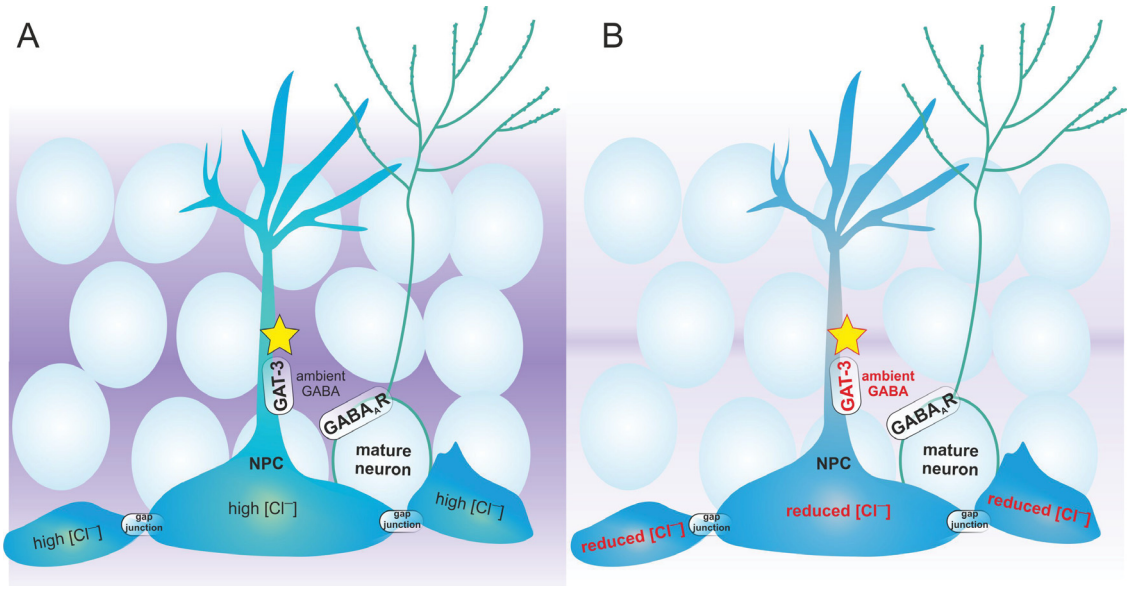


Figure 6.1: **The role of EAAT1/GLAST anion channels in the granule cell network excitability.** A: EAAT1/GLAST represented as a star regulate $[Cl^-]_{int}$ in physiological conditions. B: P290R EAAT1/GLAST cause $Cl^-$ efflux from the NPCs, facilitating GABA uptake by GAT-3. Decreased levels of ambient GABA lead to reduced neuronal tonic inhibition and may result in the granule cell network hyperexcitability.

Immunostaining of NPCs demonstrates high-affinity GAT-3, which is known to be preferentially localized on glial processes (Minelli et al., 1996; Ribak et al., 1996). Western blot analysis revealed a ~3 fold increase of GAT-3 expression in *Slc1a3*$^{P290R/+}$ hippocampi at the age of seizure onset. A possible explanation for the observed GAT-3 upregulation could be that the rise of GABA uptake-mediated $[Na^+]_{int}$ reduces the activity of the $Na^+/Ca^{2+}$ exchanger (Doengi M et

al., 2009). In turn, an elevated resting $Ca^{2+}$ level has been shown to result in the upregulation of GAT-3 in glial cells (Shigetomi et al., 2012). In later ages, the protein amount of GAT-3 decreases. This may be associated with glial cell loss in the epileptic *Slc1a3*$^{P290R/+}$ hippocampi and requires further investigation.

Gain-of-function of P290R EAAT1/GLAST anion channels has been shown to decrease $[Cl^-]_{int}$ of cerebellar Bergmann glial cells (Kovermann et al., 2020) and NPCs (unpublished data). Reduced $[Cl^-]_{int}$ in NPCs might then promote GABA uptake via GAT-3, resulting in reduced $[GABA]_{ext}$, and thereby causing a decrease in tonic conductance, as observed in *Slc1a3*$^{P290R/+}$ hippocampal granule cells (Fig. 6.1).

NPCs form a gap junction-coupled glial network with homogenous ionic concentrations and NPCs' processes wrap the excitatory synapses within the granule cell layer (Moss et al., 2016). The current study proposes a novel role of EAAT1/GLAST anion channels within the NPCs network – the control of the granule cell network excitability (Fig. 6.1).

## 6.3. Altered expression profile of the glial glutamate transporters in the *Slc1a3*$^{P290R/+}$ hippocampi

P290R leads to a lower membrane density of the human EAAT1 and decreased EAAT1/GLAST expression in heterologous expression systems and mutant cerebella (Winter et al., 2012; Kovermann et al. 2020), as well as in the mutant hippocampi. The dramatic decrease of the EAAT1/GLAST protein levels in the age of seizure onset may indicate that in addition to the reduced EAAT1/GLAST membrane expression, in *Slc1a3*$^{P290R/+}$ mice glial cells expressing EAAT1/GLAST might undergo the same fate as Bergmann glia, namely $Cl^-$ efflux-induced shrinkage and apoptosis (Kovermann et al., 2020). Although reduced EAAT1/GLAST levels were already observed during the second postnatal week, *Slc1a3*$^{P290R/+}$ animals exhibited seizures only starting from the third postnatal week. This may support the hypothesis that impaired EAAT1/GLAST glutamate uptake activity does not cause seizures since *Slc1a3*$^{-/-}$ animals were not epileptic (Watase et al., 1998).

Additionally, EAAT2/GLT-1 may compensate for the lack of EAAT1/GLAST and postpone the seizure onset. In the adult murine hippocampus EAAT1/GLAST

protein levels are ~4 times lower than EAAT2/GLT-1 (Lehre and Danboldt, 1998); studies of promoter activity show that in NPCs both EAAT1/GLAST and EAAT2/GLT-1 promoters are active and 60% of the uptake currents in these cells are carried by EAAT2/GLT-1 (Regan et al., 2007). *Slc1a3*$^{P290R/+}$ animals exhibited compensatory up-regulation of hippocampal EAAT2/GLT-1 during the second postnatal week. However, this compensation vanished in the age of seizure onset, as EAAT2/GLT-1 expression levels were similar to those observed in the WT littermates.

## 6.4 Compensatory changes in the hippocampal network of *Slc1a3*$^{P290R/+}$ mice after epilepsy

### 6.4.1 Shrinkage of the dendritic spines

After reaching the age of ~2 months surviving *Slc1a3*$^{P290R/+}$ mice did not exhibit further epileptic seizures, which suggests the development of a possible compensatory mechanism, counteracting excessive excitation in the mutant hippocampi. Seizure activity raises extracellular glutamate levels (During and Spencer, 1993; Meurs et al., 2008), possibly resulting in the restructuring of the neuronal local connectivity. In the hippocampus, the majority of excitatory connections are made at the level of dendritic spines (Harris, 1999). Spines are small protrusions, able to undergo morphological changes in response to synaptic activity (Fischer et al., 2000; Korkotian and Segal, 2001). Granule cells and CA1 pyramidal cells had reduced spine sizes in *Slc1a3*$^{P290R/+}$ animals, but unchanged spine density. Plasticity of spines is dependent on extracellular glutamate: high concentrations prevent the spine protrusion from seeking glutamate (Richards et al., 2005). The spine length controls the degree of interaction between spines and their parent dendrite: short spines show similar responses to glutamate as parent dendrites, while long spines exhibit faster and larger responses (Korkotian and Segal, 2000). Therefore, activity-dependent elimination of synaptic connections via spine retraction can account for a possible protection mechanism in hippocampal neurons from *Slc1a3*$^{P290R/+}$ animals.

### 6.4.2 Loss of VGLUT1 and VGLUT2 positive synapses

Since the results of the current study suggest that granule cells may be the first affected cells in the *Slc1a3*$^{P290R/+}$ epileptic hippocampus, I also studied their efferent projections. The multistep process of neurotransmission includes loading of the neurotransmitter into synaptic vesicle by vesicular glutamate transporters (VGLUTs). Further, alterations in the expression of the transporters directly regulate glutamate release, thereby modifying postsynaptic responses (Daniels et al., 2004; Wilson et al., 2005; Wojcik et al., 2004). Axons from granule cells form large excitatory synapses on the apical dendrites of CA3 pyramidal cells (Amaral and Witter, 1995). The CA3 region of *Slc1a3*$^{P290R/+}$ hippocampi exhibited less VGLUT1-positive release sites at ages following seizure onset. This finding may be associated with a decreased glutamate release by the mossy fibers of *Slc1a3*$^{P290R/+}$ granule cells, which could protect CA3 pyramidal cells from excessive excitation.

Additionally, the density of VGLUT2 punctae was decreased in the granule cell layer of the *Slc1a3*$^{P290R/+}$ DG. Decreased VGLUT2 expression levels, possibly resulting from seizure-induced mossy cell degeneration, have also been reported in the hippocampus of patients suffering from temporal lobe epilepsy (van Liefferinge et al., 2015).

Therefore, reduced density of VGLUT1 and VGLUT2 in paroxysmal *Slc1a3*$^{P290R/+}$ hippocampi might reduce the quantal glutamate release onto postsynaptic granule cells and CA3 pyramidal cells. This, in turn, can contribute to the decreased hippocampal excitability of the *Slc1a3*$^{P290R/+}$ mice after the paroxysmal period.

# 7 Conclusion

Glial excitatory amino acid transporters (EAATs) are dual function proteins, they are secondary active glutamate transporters and anion channels (Wadiche et al., 1995). Although EAAT1/GLAST anion channels are known to play an important role in regulating glial $[Cl^-]_{int}$ in the central nervous system (Untiet et al., 2017) and changes in channel activity lead to cerebellar degeneration (Kovermann et al., 2020), its functional importance in other brain regions remains unclear.

Mice carrying a heterozygous P290R mutation in EAAT1/GLAST exhibited epileptic seizures, whereas knock-out of EAAT1/GLAST resulted only in slight ataxia (Watase et al., 1998; Perkins et al., 2016). This work revealed, for the first time, an interplay between decreased $[Cl^-]_{int}$ in NPCs and excitability of the hippocampal neural network, that possibly cause epilepsy in mutant mice. Mutants had reduced tonic inhibition of the granule cells, followed by an increase of excitatory AMPA receptor-mediated neurotransmission in the hippocampus. Gain-of-function of P290R EAAT1/GLAST anion channels lead to lower $[Cl^-]_{int}$ in NPCs. In these cells, I confirmed the expression of GABA transporter GAT-3, which's activity is known to be dependent on $[Cl^-]_{int}$ (Zhou and Danbolt, 2013). I hypothesize that accelerated by the reduced $[Cl^-]_{int}$, GAT-3 activity may lower ambient GABA levels and consequently reduce tonic inhibition of the mutant granule cells. These findings indicate a novel role of NPCs glial network in the control of the hippocampal excitability.

My work illustrates the impact of low EAAT1/GLAST anion channel activity on the neuronal excitability of the hippocampus and highlights the importance of the optimization of glial EAATs for both effective secondary-active transport and low anion channel activity.

# 8 Acknowledgments

I am grateful to my scientific advisor Prof. Dr. Christoph Fahlke for providing me this exciting topic to investigate and multiple possibilities to present my results at national and international conferences. Amazing working conditions in his lab allowed me to perform this study with a great pleasure.

Furthermore I am immensely grateful to Peter Kovermann for being a patient, kind and creative supervisor with an outstanding musical taste.

To Miriam Engels, Jennifer Cremer, and Sabrina Buller for their collaborative effort.

To my colleagues: Steffi, Thomas, Anita, and all workers of IBI-1.

To my friends and idols: Claudia, Andrei, Daniel, Juan, Galiya, and Jan. Thank you for turning this time into an unforgettable adventure, charged with love and inspiration.

Маме и папе: спасибо за вашу безграничную веру в меня. Спасибо за Машу, с которой мы можем исследовать этот мир рука об руку.

Маше: я счастлива, что ты всегда рядом.

# 9 References


Adamczyk A., Gause C. D., Sattler R., Vidensky S., Rothstein J. D., Singer H. and Wang T. (2011). Genetic and functional studies of a missense variant in a glutamate transporter, SLC1A3, in Tourette syndrome. *Psychiatric Genetics*, 21(2), 90–97.

Altman J. (1962). Are new neurons formed in the brains of adult mammals? *Science*, 135*(*3509), 1127–8.

Amaral D. G., Scharfman H. E. and Lavenex P. (2007). The dentate gyrus: fundamental neuroanatomical organization (dentate gyrus for dummies). *Progress in Brain Research*, 163, 2–22.

Amaral D.G. and Witter M.P. (1989). The three-dimensional organization of the hippocampal formation: a review of anatomical data. *Neuroscience*, 31(3), 571–91.

Arriza J. L., Eliasof S., Kavanaugh M. P. and Amara S. G. (1997). Excitatory amino acid transporter 5, a retinal glutamate transporter coupled to a chloride conductance. *Proceedings of the National Academy of Sciences of the United States of America*, 94(8), 4155–4160.

Auger C., Kondo S. and Marty A. (1998). Multivesicular release at single functional synaptic sites in cerebellar stellate and basket cells. *Journal of Neuroscience*, 18(12), 4532–4547.

Bedner P., Dupper A., Hüttmann K., Müller J., Herde M. K., Dublin P., Deshpande T., Schramm J., Häussler U., Haas C.A., Henneberger C., Theis M. and Steinhäuser C. (2015). Astrocyte uncoupling as a cause of human temporal lobe epilepsy. *Brain*, *138*(5), 1208–1222.

Behr J., Lyson K. J., and Mody, I. (1998). Enhanced propagation of epileptiform activity through the kindled dentate gyrus. *Journal of Neurophysiology*, *79*(4), 1726–1732.

Ben-Ari Y. (2002). Excitatory actions of GABA during development: The nature of the nurture. *Nature Reviews Neuroscience*, 3(9), 728–739.

Bergles, D. E. and Jahr, C. E. (1997). Synaptic activation of glutamate transporters in hippocampal astrocytes. *Neuron*, 19(6), 1297–1308.

Blackstad, T. W. (1958). On the termination of some afferents to the hippocampus and fascia dentata. *Cells Tissues Organs*, 35(3), 202–214.

Blümcke I., Suter B., Behle K., Kuhn R., Schramm J., Elger C.E., Wiestler O.D. (2000). Loss of hilar mossy cells in Ammon's horn sclerosis. *Epilepsia*, 41 (supplement 6), 174–80.

Brunne B., Zhao S., Derouiche A., Herz J., May P., Frotscher M. & Bock H. (2010) Origin, maturation and astroglial transformation of secondary radial glial cells in the developing dentate gyrus. *Glia*, 58(13): 1553–1569.

Chadderton P., Margrie T.W. and Häusser M. (2004). Integration of quanta in cerebellar granule cells during sensory processing. *Nature* 428, 856–860.

Chaudhry F. A., Lehre K. P., Lookeren Campagne M. van, Ottersen O. P., Danbolt N. C., and Storm-Mathisen, J. (1995). Glutamate transporters in glial plasma membranes: highly differentiated localizations revealed by quantitative ultrastructural immunocytochemistry. *Neuron*, *15*(3), 711–720.

Choi K. D., Jen J. C., Choi S. Y., Shin J. H., Kim H. S., Kim H. J. and Choi J. H. (2017a). Late-onset episodic ataxia associated with *SLC1A3* mutation. *Journal of Human Genetics*, 62(3), 443–446.

Choi K. D., Kim J. S., Kim H. J., Jung I., Jeong S.H., Lee S.H., Kim D.U., Kim S.H., Choi S.Y., Shin J.H., Kim D.S., Park K.P., Kim H.S. and Choi J.H. (2017b). Genetic variants associated with episodic ataxia in Korea. *Scientific Reports*, 7(1), 1–11.

Coulter D. A. and Carlson, G. C. (2007). Functional regulation of the dentate gyrus by GABA-mediated inhibition. *Progress in Brain Research*, 163(07), 235–244.

Dagcinar A., Hilmi Kaya A., Ali Taşdemir H., Kuruoglu E., Sabancilar Z. and Sav A. (2007). A fourth ventricular ganglioneurocytoma representing with cerebellar epilepsy: A case report and review of the literature. *European Journal of Paediatric Neurology*, 11(5), 257–260.

Danbolt N. C. (2001). Glutamate uptake. *Progress in Neurobiology*, 65(1), 1–105.

Daniels R. W., Collins C. A., Gelfand M. V., Dant J., Brooks E. S., Krantz D. E. and DiAntonio A. (2004). Increased expression of the *Drosophila* vesicular glutamate transporter leads to excess glutamate release and a compensatory decrease in quantal content. *Journal of Neuroscience*, 24(46), 10466–10474.

de Vries B., Mamsa H., Stam A.H., Wan J., Bakker S.L., Vanmolkot K.R., Haan J., Terwindt G.M., Boon E.M., Howard B.D., Frants R.R., Baloh R.W., Ferrari M.D., Jen J.C. and van den Maagdenberg A.M. (2009). Episodic ataxia associated with EAAT1 mutation C186S affecting glutamate reuptake. *Archives of Neurology*, 66(1), 97–101.

DeCarolis N. A., Mechanic M., Petrik D., Carlton A., Ables J. L., Malhotra S., Bachoo R., Götz M., Lagace D.C. and Eisch A.J. (2013). In vivo contribution of nestin- and GLAST-lineage cells to adult hippocampal neurogenesis. *Hippocampus*, 23(8), 708–719.

Dibbens L. M., Feng H. J., Richards M. C., Harkin L. A., Hodgson B. L., Scott D., Jenkins M., Petrou S., Sutherland G.R., Scheffer I.E., Berkovic S.F., Macdonald R.L. and Mulley, J. C. (2004). *GABRD* encoding a protein for extra- or perisynaptic $GABA_A$ receptors is susceptibility locus for generalized epilepsies. *Human Molecular Genetics*, 13(13), 1315–1319.

Doengi M., Hirnet D., Coulon P., Pape H. C., Deitmer J. W. and Lohr C. (2009). GABA uptake-dependent $Ca^{2+}$ signaling in developing olfactory bulb astrocytes. *Proceedings of the National Academy of Sciences of the United States of America*, 106(41), 17570–17575.

Dow R. S., Fernández-Guardiola A. and Manni E. (1962). The influence of the cerebellum on experimental epilepsy. *Electroencephalography and Clinical Neurophysiology*, 14(3), 383–398.

During M. J. and Spencer D. D. (1993). Extracellular hippocampal glutamate and spontaneous seizure in the conscious human brain. *The Lancet*, 341(8861), 1607–1610.

Duveau V., Laustela S., Barth L., Gianolini F., Vogt K.E., Keist R., Chandra D., Homanics G.E., Rudolph U. and Fritschy J.M. (2011). Spatio-temporal specificity of $GABA_A$ receptor-mediated regulation of adult hippocampal neurogenesis. *European Journal of Neuroscience,* 34(3), 362–373.

Edwards F. A., Konnerth A., Sakmann B. and Takahashi T. (1989). A thin slice preparation for patch clamp recordings from neurones of the mammalian central nervous system. *Pflügers Archiv: European Journal of Physiology*, 414, 600-612.

Edwards F.A., Konnerth A., Sakmann B. (1990). Quantal analysis of inhibitory synaptic transmission in the dentate gyrus of rat hippocampal slices: a patch-clamp study. *The Journal of Physiology*, 430, 213–49.

Eriksson P. S., Perfilieva E., Björk-Eriksson T., Alborn A. M., Nordborg C., Peterson D. A., and Gage, F. H. (1998). Neurogenesis in the adult human hippocampus. *Nature Medicine*, 4(11), 1313–1317.

Eugène E., Depienne C., Baulac S., Baulac M., Fritschy J. M., Le Guern E., Miles R. and Poncer, J. C. (2007). $GABA_A$ receptor γ2 subunit mutations linked to human epileptic syndromes differentially affect phasic and tonic inhibition. *Journal of Neuroscience*, *27*(51), 14108–14116.

Eyre M. D., Renzi M., Farrant M. and Nusser Z. (2012). Setting the time course of inhibitory synaptic currents by mixing multiple $GABA_A$ receptor α subunit isoforms. *Journal of Neuroscience*, 32(17), 5853–5867.

Fairman W.A., Vandenberg R.J., Arriza J.L., Kavanaugh M.P. and Amara S.G. (1995). An excitatory amino-acid transporter with properties of a ligand-gated chloride channel. *Nature*, 375(6532), 599–603.

Farrant M. and Kaila K. (2007). The cellular, molecular and ionic basis of $GABA_A$ receptor signalling. *Progress in Brain Research*, 160, 59–87.

Feng H. J., Kang J. Q., Song L., Dibbens L., Mulley J. and Macdonald R. L. (2006). δ subunit susceptibility variants E177A and R220H associated with complex epilepsy alter channel gating and surface expression of α4β2δ $GABA_A$ receptors. *Journal of Neuroscience*, 26(5), 1499–1506.

Fiala J. C. (2005). Reconstruct: A free editor for serial section microscopy. *Journal of Microscopy*, 218(1), 52–61.

Fischer M., Kaech S., Wagner U., Brinkhaus H. and Matus A. (2000). Glutamate receptors regulate actin-based plasticity in dendritic spines. *Nature Neuroscience*, 3(9), 887–894.

Fremeau R. T., Troyer M. D., Pahner I., Nygaard G. O., Tran C. H., Reimer R. J., Bellocchio E.E., Fortin D., Storm-Mathisen J. and Edwards R. H. (2001). The

expression of vesicular glutamate transporters defines two classes of excitatory synapse. *Neuron*, 31(2), 247–260.

Fremeau R. T., Kam K., Qureshi Y., Johnson J., Copenhagen D. R., Storm-Mathisen J., Chaudhry F.A., Nicoll R.A. and Edwards, R.H. (2004). Vesicular glutamate transporters 1 and 2 target to functionally distinct synaptic release sites. *Science*, 304(5678), 1815–1819.

French J.A., Krauss G.L., Biton V., Squillacote D., Yang H., Laurenza A., Kumar D., Rogawski M.A. (2012). Adjunctive perampanel for refractory partial-onset seizures: randomized phase III study 304. *Neurology*, 79(6), 589–96

French, J. A., Krauss, G. L., Wechsler, R. T., Wang, X. F., Diventura, B., Brandt, C., Trinka E., O'Brien T.J., Laurenza A., Patten A. and Bibbiani, F. (2015). Perampanel for tonic-clonic seizures in idiopathic generalized epilepsy. *Neurology*, 85(11), 950–957.

Frerking M., Borges S. and Wilson M. (1995). Variation in GABA mini amplitude is the consequence of variation in transmitter concentration. *Neuron*, 15(4), 885–895.

Furuta A., Rothstein J. D. and Martin J. L. (1997). Glutamate transporter protein subtypes are expressed differentially during rat cns development. *Journal of Neuroscience*, 17(21), 8363–8375.

Ge S., Goh E. L. K., Sailor K. A., Kitabatake Y., Ming G. L. and Song H. (2006). GABA regulates synaptic integration of newly generated neurons in the adult brain. *Nature*, 439(7076), 589–593.

Gilley J.A. and Kernie S.G. (2011). Excitatory amino acid transporter 2 and excitatory amino acid transporter 1 negatively regulate calcium-dependent proliferation of hippocampal neural progenitor cells and are persistently upregulated after injury. *European Journal of Neuroscience,* 34(11), 1712–1723.

Glykys J. and Mody I. (2007). The main source of ambient GABA responsible for tonic inhibition in the mouse hippocampus. *Journal of Physiology*, 582(3), 1163–1178.

Gupta V., Garg A., Chandra S., Sharma M.C., Gaikwad S.B., Gulati S. and Mishra N.K. (2003). Cerebellar epilepsy: a case report of a cerebellar gangliomatous hamartoma. *The Neuroradiology Journal*, 16, 784–787.

Hagemann G., Lemieux L., Free S. L., Krakow K., Everitt A. D., Kendall B. E., Stevens J.M. and Shorvon S. D. (2002). Cerebellar volumes in newly diagnosed and chronic epilepsy. *Journal of Neurology*, 249(12), 1651–1658.

Halasy K., Hajszan T., Kovćs É. G., Lam T. T. and Leranth C. (2004). Distribution and origin of vesicular glutamate transporter 2-immunoreactive fibers in the rat hippocampus. *Hippocampus*, 14(7), 908–918.

Hamann M., Rossi D. J. and Attwell D. (2002). Tonic and spillover inhibition of granule cells control information flow through cerebellar cortex. *Neuron*, 33(4), 625–633.

Harris K. M. (1999). Structure, development, and plasticity of dendritic spines. *Current Opinion in Neurobiology*, 9(3), 343–348.

Heinemann U., Beck H., Dreier J.P., Ficker E., Stabel J., Zhang C.L. (1992). The dentate gyrus as a regulated gate for the propagation of epileptiform activity. *Epilepsy research. Supplement,* 7, 273–80.

Holmseth, S., Dehnes, Y., Huang, Y. H., Follin-Arbelet, V. V., Grutle, N. J., Mylonakou, M. N., Plachez C., Zhou Y., Furness D.N., Bergles D.E., Lehre K.P. and Danbolt N. C. (2012). The density of EAAC1 (EAAT3) glutamate transporters expressed by neurons in the mammalian CNS. *Journal of Neuroscience*, 32(17), 6000–6013.

Hotzy J., Schneider N., Kovermann P. and Fahlke, C. (2013). Mutating a conserved proline residue within the trimerization domain modifies $Na^+$ binding to excitatory amino acid transporters and associated conformational changes. *Journal of Biological Chemistry*, 288(51), 36492–36501.

Hutton J. T., Frost J. D. and Foster J. (1972). The influence of the cerebellum in cat penicillin epilepsy. *Epilepsia*, 13(3), 401–408.

Iwama K., Iwata A., Shiina M., Mitsuhashi S., Miyatake S., Takata A., Miyake N., Ogata K., Ito S., Mizuguchi T. and Matsumoto, N. (2017). A novel mutation in *SLC1A3* causes episodic ataxia. *Journal of Human Genetics*, 63(2), 207–211.

Jagasia R., Steib K., Englberger E., Herold S., Faus-Kessler T., Saxe M., Gage F.H., Song H. and Lie D.C. (2009). GABA-cAMP response element-binding protein signaling regulates maturation and survival of newly generated neurons in the adult hippocampus. *Journal of Neuroscience*, 29(25), 7966–7977.

Jen J. C., Wan J., Palos T. P., Howard B. D. and Baloh R. W. (2005). Mutation in the glutamate transporter EAAT1 causes episodic ataxia, hemiplegia, and seizures. *Neurology*, 65(4), 529–534.

Jensen A. A., Fahlke C., Bjørn-Yoshimoto W. E. and Bunch L. (2015). Excitatory amino acid transporters: Recent insights into molecular mechanisms, novel modes of modulation and new therapeutic possibilities. *Current Opinion in Pharmacology*, 20, 116–123.

Jungblut M., Tiveron M. C., Barral S., Abrahamsen B., Knöbel S., Pennartz S., Schmitz J., Perraut M., Pfrieger F.W., Stoffel W., Cremer H. and Bosio, A. (2012). Isolation and characterization of living primary astroglial cells using the new GLAST-specific monoclonal antibody ACSA-1. *Glia*, 60(6), 894–907.

Kaneko T. and Fujiyama F. (2002). Complementary distribution of vesicular glutamate transporters in the central nervous system. *Neuroscience Research*, 42(4), 243–250.

Kempermann G., Kuhn H. G. and Gage, F. H. (1997). More hippocampal neurons in adult mice living in an enriched environment. *Nature*, 386, 493–495.

Kielbinski M., Gzielo K. and Soltys Z. (2016). Roles for astrocytes in epilepsy: insights from malformations of cortical development. *Neuropathology and Applied Neurobiology*, 42(7), 593–606.

Kienzler F., Norwood B.A. and Sloviter R.S. (2009) Hippocampal injury, atrophy, synaptic reorganization, and epileptogenesis after perforant pathway stimulation-

induced status epilepticus in the mouse. *The Journal of Comparative Neurology*, 515, 181–196.

Korkotian E. and Segal M. (2000). Structure-function relations in dendritic spines: Is size important? *Hippocampus*, 10(5), 587–595.

Korkotian E. and Segal M. (2001). Regulation of dendritic spine motility in cultured hippocampal neurons. *Journal of Neuroscience*, 21(16), 6115–6124.

Kovermann P., Hessel M., Kortzak D., Jen J. C., Koch J., Fahlke, C. and Freilinger T. (2017). Impaired $K^+$ binding to glial glutamate transporter EAAT1 in migraine. *Scientific Reports*, 7(1), 1–10.

Kovermann P., Untiet V., Kolobkova Y., Engels M., Baader S., Schilling K. and Fahlke C. (2020). Increased glutamate transporter-associated anion currents cause glial apoptosis in episodic ataxia 6. *Brain Communications,* accepted 2 February 2020.

Krook-Magnuson E., Szabo G. G., Armstrong C., Oijala M. and Soltesz, I. (2014). Cerebellar directed optogenetic intervention inhibits spontaneous hippocampal seizures in a mouse model of temporal lobe epilepsy. *ENeuro*, 1(1).

Kuhn H. G., Dickinson-Anson H. and Gage F. H. (1996). Neurogenesis in the dentate gyrus of the adult rat: age-related decrease of neuronal progenitor proliferation. *Journal of Neuroscience*, 16(6), 2027–2033.

Kunze A., Congreso M. R., Hartmann C., Wallraff-Beck A., Hüttmann K., Bedner P., Requardt R., Seifert G., Redecker C., Willecke K., Hofmann A., Pfeifer A., Theis M. and Steinhäuser C. (2009). Connexin expression by radial glia-like cells is required for neurogenesis in the adult dentate gyrus. *Proceedings of the National Academy of Sciences of the United States of America*, 106(27), 11336–11341.

Lee A., Anderson A. R., Stevens M. G., Beasley S., Barnett N. L. and Pow, D. V. (2013). Excitatory amino acid transporter 5 is widely expressed in peripheral tissues. *European Journal of Histochemistry*, 57(1), 66–71.

Lehre K. P. and Danbolt N. C. (1998). The number of glutamate transport subtype molecules at glutamatergic synapses: chemical and stereological quantification in young adult rat brain. *Journal of Neuroscience*, 18(21), 8751–8757.

Levy, L. M., Warr, O. and Attwell, D. (1998). Stoichiometry of the glial glutamate transporter GLT-1 expressed inducibly in a Chinese hamster ovary cell line selected for low endogenous $Na^+$-dependent glutamate uptake. *Journal of Neuroscience*, 18(23), 9620–9628.

Lindquist C. E. L. and Birnir B. (2006). Graded response to GABA by native extrasynaptic $GABA_A$ receptors. *Journal of Neurochemistry*, 97(5), 1349–1356.

Lothman E.W., Stringer J.L., Bertram E.H. (1992). The dentate gyrus as a control point for seizures in the hippocampus and beyond. *Epilepsy research. Supplement,* 7: 301–13.

LoTurco J. J., Owens D. F., Heath M. J. S., Davis M. B. E. and Kriegstein, A. R. (1995). GABA and glutamate depolarize cortical progenitor cells and inhibit DNA synthesis. *Neuron*, 15(6), 1287–1298.

Lu Y., Zhong C., Wang L., Wei P., He W., Huang K., Zhang Y., Zhan Y., Feng G. and Wang, L. (2016). Optogenetic dissection of ictal propagation in the hippocampal-entorhinal cortex structures. *Nature Communications*, 7, doi:10.1038/ncomms10962.

Machtens, J. P., Kortzak, D., Lansche, C., Leinenweber, A., Kilian, P., Begemann, B., Zachariae U., Ewers D., de Groot B.L., Briones R. and Fahlke, C. (2015). Mechanisms of anion conduction by coupled glutamate transporters. *Cell*, 160(3), 542–553.

Maguire J. L., Stell B. M., Rafizadeh M. and Mody I. (2005). Ovarian cycle-linked changes in $GABA_A$ receptors mediating tonic inhibition alter seizure susceptibility and anxiety. *Nature Neuroscience*, 8(6), 797–804.

Martin L. J., Bonin R. P. and Orser B. A. (2009). The physiological properties and therapeutic potential of α5-$GABA_A$ receptors. *Biochemical Society Transactions*, 37(6), 1334–1337.

Martins W. A., Paglioli E., Hemb M. and Palmini, A. (2016). Dysplastic cerebellar epilepsy: complete seizure control following resection of a ganglioglioma. *Cerebellum*, 15(4), 535–541.

Melzer N., Biela A. and Fahlke C. (2003) Glutamate modifies ion conduction and voltage-dependent gating of excitatory amino acid transporter-associated anion channels. *Journal of Biological Chemistry*, 278, 50112–50119

Meurs A., Clinckers R., Ebinger G., Michotte Y. and Smolders I. (2008). Seizure activity and changes in hippocampal extracellular glutamate, GABA, dopamine and serotonin. *Epilepsy Research*, 78(1), 50–59.

Minelli A., DeBiasi S., Brecha N. C., Zuccarello L. V. and Conti F. (1996). GAT-3, a high-affinity GABA plasma membrane transporter, is localized to astrocytic processes, and it is not confined to the vicinity of GABAergic synapses in the cerebral cortex. *Journal of Neuroscience*, 16(19), 6255–6264.

Mitchell S. J. and Silver R. A. (2003). Shunting inhibition modulates neuronal gain during synaptic excitation. *Neuron*, 38(3), 433–445.

Miyazaki T., Yamasaki M., Hashimoto K., Kohda K., Yuzaki M., Shimamoto K., Tanaka K., Kano M. and Watanabe M. (2017). Glutamate transporter GLAST controls synaptic wrapping by Bergmann glia and ensures proper wiring of Purkinje cells. *Proceedings of the National Academy of Sciences of the United States of America*, 114(28), 7438–7443.

Mori T., Tanaka K., Buffo A., Wurst W., Kühn R. and Götz M. (2006). Inducible gene deletion in astroglia and radial glia – a valuable tool for functional and lineage analysis. *Glia*, 54(1), 21–34.

Moss J., Gebara E., Bushong E. A., Sánchez-Pascual I., O'Laoi R., El M'Gharia I., Kocher-Braissant J., Ellisman M.H. and Toni N. (2016). Fine processes of Nestin-GFP-

positive radial glia-like stem cells in the adult dentate gyrus ensheathe local synapses and vasculature. *Proceedings of the National Academy of Sciences of the United States of America*, 113(18), E2536–E2545.

Mulley J. C., Scheffer I. E., Harkin L. A., Berkovic S. F. and Dibbens L. M. (2005). Susceptibility genes for complex epilepsy. *Human Molecular Genetics*, 14 (supplement 2), 243–249.

Nusser Z., Cull-Candy S. and Farrant M. (1997). Differences in synaptic $GABA_A$ receptor number underlie variation in GABA mini amplitude. *Neuron*, 19(3), 697–709.

Nusser Z. and Mody I. (2002). Selective modulation of tonic and phasic inhibitions in dentate gyrus granule cells. *Journal of Neurophysiology*, 87(5), 2624–2628.

Owens D. F., Boyce L. H., Davis M. B. E. and Kriegstein A. R. (1996). Excitatory GABA responses in embryonic and neonatal cortical slices demonstrated by gramicidin perforated-patch recordings and calcium imaging. *Journal of Neuroscience*, 16(20), 6414–6423.

Parinejad N., Peco E., Ferreira T., Stacey S. M., and Van Meyel, D. J. (2016). Disruption of an EAAT-mediated chloride channel in a *Drosophila* model of ataxia. *Journal of Neuroscience*, 36(29), 7640–7647.

Pekny M., Pekna M., Messing A., Steinhäuser C., Lee J. M., Parpura V., Hol E.M., Sofroniew M.V. and Verkhratsky A. (2016). Astrocytes: a central element in neurological diseases. *Acta Neuropathologica*, 131(3), 323–345.

Peng Z., Huang C. S., Stell B. M., Mody I. and Houser C. R. (2004). Altered expression of the δ subunit of the $GABA_A$ receptor in a mouse model of temporal lobe epilepsy. *Journal of Neuroscience*, 24(39), 8629–8639.

Perkins E. M., Suminaite D., Clarkson Y. L., Lee S. K., Lyndon A. R., Rothstein J. D. And Jackson M. (2016). Posterior cerebellar Purkinje cells in an SCA5/SPARCA1 mouse model are especially vulnerable to the synergistic effect of loss of β-III spectrin and GLAST. *Human Molecular Genetics*, 25(20), 4448–4461.

Pirker S., Schwarzer C., Wieselthaler A., Sieghart W., Sperk G. (2000). $GABA_A$ receptors: immunocytochemical distribution of 13 subunits in the adult rat brain. *Neuroscience*, 101(4), 815–50.

Pyle A., Smertenko T., Bargiela D., Griffin H., Duff J., Appleton M., Douroudis K., Pfeffer G., Santibanez-Koref M., Eglon G., Yu-Wai-Man P., Ramesh V., Horvath R. and Chinnery P.F. (2015). Exome sequencing in undiagnosed inherited and sporadic ataxias. *Brain*, 138(Pt 2), 276–83.

Raponi E., Agenes F., Delphin C., Assard N., Baudier J., Legraverend C. and Deloulme J.C. (2007). S100B expression defines a state in which GFAP-expressing cells lose their neural stem cell potential and acquire a more mature developmental stage. *Glia*, 55(2),165–77.

Rauen T., Rothstein J. D. and Wässle H. (1996). Differential expression of three glutamate transporter subtypes in the rat retina. *Cell and Tissue Research*, 286(3), 325–336.

Regan M. R., Huang Y. H., Yu S. K., Dykes-Hoberg M. I., Jin L., Watkins A. M., Bergles D.E. and Rothstein J. D. (2007). Variations in promoter activity reveal a differential expression and physiology of glutamate transporters by glia in the developing and mature CNS. *Journal of Neuroscience*, 27(25), 6607–6619.

Ribak C. E., Tong W. M. Y. and Brecha N. C. (1996). GABA plasma membrane transporters, GAT-1 and GAT-3, display different distributions in the rat hippocampus. *Journal of Comparative Neurology*, 367(4), 595–606.

Richards D.A., Mateos J.M., Hugel S., de Paola V., Caroni P., Gähwiler B. H. and Mckinney R. A. (2005). Glutamate induces the rapid formation of spine head protrusions in hippocampal slice cultures. *Proceedings of the National Academy of Sciences of the United States of America*, 102(17).

Richerson G. B. and Wu Y. (2003). Dynamic equilibrium of neurotransmitter transporters: not just for reuptake anymore. *Journal of Neurophysiology*, 90(3), 1363–1374.

Rogawski M.A. (2013). AMPA Receptors as a molecular target in epilepsy therapy. *Acta neurologica Scandinavica. Supplementum*, 197, 9–18.

Rothstein J. D., Martin L., Levey A. I., Dykes-Hoberg M., Jin, L., Wu, D., Nash N. and Kuncl R. W. (1994). Localization of neuronal and glial glutamate transporters. *Neuron*, 13(3), 713–725.

Roy N. S., Wang S., Jiang L., Kang J., Benraiss A., Harrison-Restelli C., Fraser R.A., Couldwell W.T., Kawaguchi A., Okano H., Nedergaard M. and Goldman S. A. (2000). In vitro neurogenesis by progenitor cells isolated from the adult human hippocampus. *Nature Medicine*, 6(3), 271–277.

Russell J. M. (2000). Sodium-potassium-chloride cotransport. *Physiological Reviews*, 80(1), 211–276.

Schneider N., Cordeiro S., Machtens J.P., Braams S., Rauen T. and Fahlke C. (2014) Functional properties of the retinal glutamate transporters GLT-1c and EAAT5. *J. Biol. Chem*, 289, 1815–1824.

Schreiner A. E., Durry S., Aida T., Stock M. C., Rüther U., Tanaka K., Rose C.R. and Kafitz K.W. (2013). Laminar and subcellular heterogeneity of GLAST and GLT-1 immunoreactivity in the developing postnatal mouse hippocampus. *Journal of Comparative Neurology*, 522(1), 204–224.

Semyanov A., Walker M. C. and Kullmann D. M. (2003). GABA uptake regulates cortical excitability via cell type-specific tonic inhibition. *Nature Neuroscience*, *6*(5), 484–490.

Shibata T., Yamada K., Watanabe M., Ikenaka K., Wada K., Tanaka K., and Inoue Y. (1997). Glutamate transporter GLAST is expressed in the radial glia-astrocyte lineage of developing mouse spinal cord. *Journal of Neuroscience*, 17(23), 9212–9219.

Shigetomi E., Tong X., Kwan K.Y., Corey D.P. and Khakh B.S. (2012). TRPA1 channels regulate astrocyte resting calcium levels and inhibitory synapse efficacy via GAT-3, *Nature Neuroscience,* 15(1), 70–80.

Soussi R., Boulland J.L., Bassot E., Bras H., Coulon P., Chaudhry F.A., Storm-Mathisen J., Ferhat L. and Esclapez M. (2015). Reorganization of supramammillary-hippocampal pathways in the rat pilocarpine model of temporal lobe epilepsy: evidence for axon terminal sprouting. *Brain Structure and Function*, 220(4), 2449–68.

Spigelman I., Li Z., Banerjee P. K., Mihalek R. M., Homanics G. E. and Olsen R. W. (2002). Behavior and physiology of mice lacking the $GABA_A$-receptor δ subunit. *Epilepsia*, 43 (supplement 5), 3–8.

Stell B. M., Brickley S. G., Tang C. Y., Farrant M. and Mody I. (2003). Neuroactive steroids reduce neuronal excitability by selectively enhancing tonic inhibition mediated by δ subunit-containing $GABA_A$ receptors. *Proceedings of the National Academy of Sciences of the United States of America*, 100 (supplement 2), 14439–14444.

Strazzer S., Zucca C., and Fiocchi I. (2006) Epilepsy and neuropsychologic deficit in a child with cerebellar astrocytoma. *Journal of Child Neurology*, 21(9): 817–820.

Sun B., Halabisky B., Zhou Y., Palop J. J., Yu G., Mucke L., Gan L. (2009). Imbalance between GABAergic and glutamatergic transmission impairs adult neurogenesis in an animal model of Alzheimer's disease. *Cell Stem Cell*. 5(6), 624–633.

Sun L., Yu Z., Wang W. and Liu X. (2012). Both NKCC1 and anion exchangers contribute to $Cl^-$ accumulation in postnatal forebrain neuronal progenitors. *European Journal of Neuroscience*, 35(5), 661–672.

Sutherland M. L., Delaney T. A. and Noebels J. L. (1996). Glutamate transporter mRNA expression in proliferative zones of the developing and adult murine CNS. *Journal of Neuroscience*, 16(7), 2191–2207.

Torres G. E. and Amara S. G. (2007). Glutamate and monoamine transporters: new visions of form and function. *Current Opinion in Neurobiology*, 17(3), 304–312.

Tozuka Y., Fukuda S., Namba T., Seki T. and Hisatsune T. (2005). GABAergic excitation promotes neuronal differentiation in adult hippocampal progenitor cells. *Neuron*, 47(6), 803–815.

Tse D. Y., Chung I. and Wu S. M. (2014). Pharmacological inhibitions of glutamate transporters EAAT1 and EAAT2 compromise glutamate transport in photoreceptor to ON-bipolar cell synapses. *Vision Research*, 103(1), 49–62.

Tzingounis A. V., and Wadiche J. I. (2007). Glutamate transporters: Confining runaway excitation by shaping synaptic transmission. *Nature Reviews Neuroscience*, 8(12), 935–947.

Untiet V., Kovermann P., Gerkau N. J., Gensch T., Rose C. R. and Fahlke C. (2017). Glutamate transporter-associated anion channels adjust intracellular chloride concentrations during glial maturation. *Glia*, 65(2), 388–400.

van Amen-Hellebrekers C. J. M., Jansen S., Pfundt R., Schuurs-Hoeijmakers J. H., Koolen D. A., Marcelis C. L., de Leeuw N., and de Vries, B. B. (2016). Duplications of *SLC1A3* associated with ADHD and autism. *European Journal of Medical Genetics*, 59(8), 373–376.

van Liefferinge J., Jensen C. J., Albertini G., Bentea E., Demuyser T., Merckx E., Aronica E., Smolders I. and Massie A. (2015). Altered vesicular glutamate transporter expression in human temporal lobe epilepsy with hippocampal sclerosis. *Neuroscience Letters*, 590, 184–188.

Vandenberg, R. J., & Ryan, R. M. (2013). Mechanisms of glutamate transport. *Physiological Reviews*, 93(4), 1621–1657.

Verkman A. S., Sellers M. C., Chao A. C., Leung T. and Ketcham, R. (1989). Synthesis and characterization of improved chloride-sensitive fluorescent indicators for biological applications. *Analytical Biochemistry*, 178(2), 355–361.

Wadiche J. I., Arriza J. L., Amara S. G. and Kavanaugh M. P. (1995). Kinetics of a human glutamate transporter. *Neuron*, 14(5), 1019–1027.

Watase K., Hashimoto K., Kano M., Yamada K., Watanabe M., Inoue Y., Okuyama S., Sakagawa T., Ogawa S., Kawashima N., Hori S., Takimoto M., Wada K., and Tanaka K. (1998). Motor discoordination and increased susceptibility to cerebellar injury in GLAST mutant mice. *European Journal of Neuroscience*, 10(3), 976–988.

Williams S. R., Buhl E. H. and Mody I. (1998). The dynamics of synchronized neurotransmitter release determined from compound spontaneous IPSCs in rat dentate granule neurones in vitro. *Journal of Physiology*, 510(2), 477–497.

Wilson N. R., Kang J., Hueske E. V., Leung T., Varoqui H., Murnick J. G., Erickson J.D. and Liu G. (2005). Presynaptic regulation of quantal size by the vesicular glutamate transporter VGLUT1. *Journal of Neuroscience*, 25(26), 6221–6234.

Winter N., Kovermann P., and Fahlke, C. (2012). A point mutation associated with episodic ataxia 6 increases glutamate transporter anion currents. *Brain*, 135(11), 3416–3425.

Witter M. P. (2007). Intrinsic and extrinsic wiring of CA3: indications for connectional heterogeneity. *Learning and Memory*, 14(11), 705–713.

Wlodarczyk A. I., Sylantyev S., Herd M. B., Kersanté F., Lambert J. J., Rusakov D. A., Linthorst A.C., Semyanov A., Belelli D., Pavlov I., Walker M.C. and Walker M. C. (2013). GABA-independent $GABA_A$ receptor openings maintain tonic currents. *Journal of Neuroscience*, 33(9), 3905–3914.

Wojcik S. M., Rhee J. S., Herzog E., Sigler A., Jahn R., Takamori S., Brose N. and Rosenmund C. (2004). An essential role for vesicular glutamate transporter 1

(VGLUT1) in postnatal development and control of quantal size. *Proceedings of the National Academy of Sciences of the United States of America*, 101(18), 7158–7163.

Yamada K., Watanabe M., Shibata T., Tanaka K., Wada K., and Inoue Y. (1996). EAAT4 is a post-synaptic glutamate transporter at Purkinje cell synapses. *NeuroReport*, 7(12), 2013–7.

Zaqout S. and Kaindl A. M. (2016). Golgi-Cox Staining step by step. *Frontiers in Neuroanatomy*, 10, 1–7.

Zerangue, N., and Kavanaugh, M. P. (1996). Flux coupling in a neuronal glutamate transporter. *Nature*, 383(6601), 634–637.

Zhang N., Wei Z., Mody I. and Houser, C. R. (2007). Altered localization of $GABA_A$ receptor subunits on dentate granule cell dendrites influences tonic and phasic inhibition in a mouse model of epilepsy. *Journal of Neuroscience*, 27(28), 7520–7531.

Zilles K., Schleicher A., Palomero-Gallagher N. and Amunts K. (2002a). Quantitative analysis of cyto- and receptor architecture of the human brain. *Brain mapping: the methods*. 573–602.

Zilles K., Palomero-Gallagher N., Grefkes C., Scheperjans F., Boy C., Amunts K. and Schleicher A. (2002b). Architectonics of the human cerebral cortex and transmitter receptor fingerprints: reconciling functional neuroanatomy and neurochemistry. *European Neuropsychopharmacology*, 12(6), 587–599.

Zhou, Y., & Danbolt, N. C. (2013). GABA and glutamate transporters in brain. *Frontiers in Endocrinology*, 4, 1–14.

# 10 Publications

During my Ph.D. studies I contributed to the peer-reviewed publication:

Peter Kovermann*, Verena Untiet*, Yulia Kolobkova*, Miriam Engels, Stephan Baader, Karl Schilling, and Christoph Fahlke.

**Increased glutamate transporter-associated anion currents cause glial apoptosis in episodic ataxia 6.**

In: *Brain Communications*, accepted 2.02.2020.

* these authors contributed equally

Author‘s contribution statement: I contributed the patch-clamp recordings and the analysis of the $Cl^-$ current recordings in Bergmann glial cells. I performed and analyzed western blots of cerebellar lysates.

# 11 Abbreviations

| | |
|---|---|
| A | Ampere |
| AB | Antibody |
| AMPA | α-amino-3-hydroxy-5-methylisoxazole-4-propionic acid |
| BLBP | Brain lipid-binding protein |
| bp | Base pairs |
| BCA | Bicinchoninic Acid |
| BSA | Bovine serum albumin |
| °C | Celsius |
| CI | Confidence interval (95 %) |
| $[Cl^-]_{int}$ | Intracellular chloride concentration |
| CA | Cornu Ammonis |
| $CO_2$ | Carbon dioxide |
| DG | Dentate gyrus |
| EA6 | Episodic ataxia subtype 6 |
| EAAT | Excitatory amino acid transporter |
| ES | Embryonic stem (cells) |
| FZJ | Forschungszentrum Jülich GmbH |
| CNQX | Cyanquixaline |
| GABA | Gamma amino isobutyric acid |
| $[GABA]_{ext}$ | Extracellular gamma amino isobutyric acid concentration |
| GAT | GABA transporter |
| GLAST | Mouse EAAT1 |
| GLT-1 | Mouse EAAT2 |
| HRP | Horseradish peroxidase |
| KO | Knock-out |
| mGluR | Metabotropic glutamate receptor |
| mEPSCs | Miniature excitatory postsynaptic currents |

| | |
|---|---|
| mIPSCs | Miniature inhibitory postsynaptic currents |
| MQAE | 1-(Ethoxycarbonylmethyl)-6-methoxyquinolinuim bromide |
| NMDA | N-methyl-D-aspartate |
| NPC | Neural progenitor cell |
| p | Level of significance |
| P | Postnatal day |
| P290R | Proline at position 290 substituted by arginine |
| PBS | Phosphate buffered saline |
| PCR | Polymerase chain reaction |
| PFA | Paraformaldehyde |
| PTX | Picrotoxin |
| RT | Room temperature |
| RCF | Relative centrifugal force |
| SDS | Sodium dodecyl sulfate |
| SLC | Solute carrier family |
| $Slc1a3^{-/-}$ | EAAT1/GLAST (Slc1a3) knock-out |
| SR101 | Sulforhodamine 101 |
| Ω | Ohm |
| V | Volt |
| v/v | Volume/volume |
| VGLUT1 | Vesicular glutamate transporter |
| WT | Wild type |
| w/v | Weight/volume |

# 12 Eidesstattliche Versicherung

Ich versichere an Eides statt, dass die Dissertation von mir selbstständig und ohne unzulässige fremde Hilfe unter Beachtung der „Grundsätze zur Sicherung guter wissenschaftlicher Praxis an der Heinrich-Heine-Universität Düsseldorf“ erstellt worden ist.

---

Jülich, 13.02.2020 Iuliia Kolobkova